Article

Neuron

# Mechanisms Underlying Microbial-Mediated Changes in Social Behavior in Mouse Models of Autism Spectrum Disorder

## Graphical Abstract

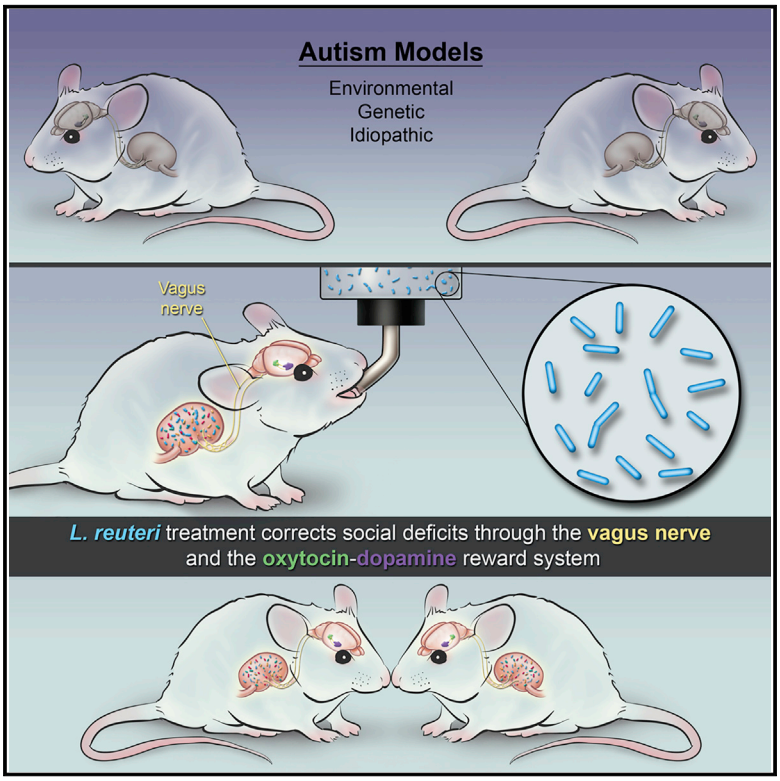


## Authors

Martina Sgritta, Sean W. Dooling, Shelly A. Buffington, Eric N. Momin, Michael B. Francis, Robert A. Britton, Mauro Costa-Mattioli

## Correspondence

costamat@bcm.edu

## In Brief

Precision microbial-based therapy rescues social deficits in genetic, environmental, and idiopathic mouse models of ASD. This rescue depends upon the vagus nerve as well as the oxytocinergic and dopaminergic signaling in the brain.

## Highlights

- Treatment with *L. reuteri* rescues social deficits in several ASD mouse models
- *L. reuteri* reverses social deficits via the vagus nerve
- *L. reuteri* reverses social deficits even in germ-free mice
- OXTR inhibition prevents *L. reuteri*'s effects on social behavior and VTA plasticity

Sgritta et al., 2019, Neuron *101*, 1–14
January 16, 2019 
https://doi.org/10.1016/j.neuron.2018.11.018

CellPress

Please cite this article in press as: Sgritta et al., Mechanisms Underlying Microbial-Mediated Changes in Social Behavior in Mouse Models of Autism Spectrum Disorder, Neuron (2018), https://doi.org/10.1016/j.neuron.2018.11.018

Neuron
Article



# Mechanisms Underlying Microbial-Mediated Changes in Social Behavior in Mouse Models of Autism Spectrum Disorder

Martina Sgritta,[1,2] Sean W. Dooling,[1,2,3] Shelly A. Buffington,[1,2] Eric N. Momin,[4] Michael B. Francis,[1,2] Robert A. Britton,[5] and Mauro Costa-Mattioli[1,2,3,6,*]
[1]Department of Neuroscience, Baylor College of Medicine, Houston, TX 77030, USA
[2]Memory and Brain Research Center, Baylor College of Medicine, Houston, TX 77030, USA
[3]Department of Molecular & Human Genetics, Baylor College of Medicine, Houston, TX 77030, USA
[4]Department of Neurosurgery, Baylor College of Medicine, Houston, TX 77030, USA
[5]Department of Molecular Virology and Microbiology, Baylor College of Medicine, Houston, TX 77030, USA
[6]Lead Contact
*Correspondence: costamat@bcm.edu
https://doi.org/10.1016/j.neuron.2018.11.018

## SUMMARY

**Currently, there are no medications that effectively treat the core symptoms of Autism Spectrum Disorder (ASD). We recently found that the bacterial species *Lactobacillus (L.) reuteri* reverses social deficits in maternal high-fat-diet offspring. However, whether the effect of *L. reuteri* on social behavior is generalizable to other ASD models and its mechanism(s) of action remains unknown. Here, we found that treatment with *L. reuteri* selectively rescues social deficits in genetic, environmental, and idiopathic ASD models. Interestingly, the effects of *L. reuteri* on social behavior are not mediated by restoring the composition of the host's gut microbiome, which is altered in all of these ASD models. Instead, *L. reuteri* acts in a vagus nerve-dependent manner and rescues social interaction-induced synaptic plasticity in the ventral tegmental area of ASD mice, but not in oxytocin receptor-deficient mice. Collectively, treatment with *L. reuteri* emerges as promising non-invasive microbial-based avenue to combat ASD-related social dysfunction.**

## INTRODUCTION

The prevalence of autism spectrum disorder (ASD), which is influenced by both genetic and environmental factors (Hallmayer et al., 2011; Kim and Leventhal, 2015), continues to increase worldwide (Baio et al., 2018; Kawa et al., 2017). However, effective treatments for ASD remain elusive. Defined as a heterogeneous neurodevelopmental disorder, ASD is characterized by social deficits, repetitive behaviors, and language difficulties (American Psychiatric Association, 2013). In addition to these core symptoms, ASD patients are often afflicted with gastrointestinal (GI) issues (Holingue et al., 2018; McElhanon et al., 2014; Vuong and Hsiao, 2017). In fact, children with ASD are 3.5 times more likely to suffer from GI disorders than children without developmental disorders (Schieve et al., 2012). Moreover, GI problems have been associated with changes in the microbial communities inhabiting the gut of ASD individuals (Ding et al., 2017; Vuong and Hsiao, 2017).

Studies in animal models have shown that gut microbes can modulate central nervous system (CNS)-driven behaviors in a very powerful way (Borre et al., 2014; Sharon et al., 2016; Vuong et al., 2017). Recently, in mice, we showed that maternal high-fat diet (MHFD) induces social deficits and a change in the gut microbiota of offspring that is characterized by a reduction of the commensal bacterial species *L. reuteri* (Buffington et al., 2016). Consistent with these data, HFD-induced obesity in adult mice also leads to a reduction in the levels of *L. reuteri* (Sun et al., 2016). More importantly, selective treatment with *L. reuteri* reverses the social deficits in MHFD offspring (Buffington et al., 2016). However, whether *L. reuteri* can also rescue the social deficits of ASD models with different underlying etiologies remains unknown. Here, we first studied whether *L. reuteri* is able to reverse the social deficits in other mouse models of ASD. Surprisingly, we found that microbial treatment with this single bacterial species rescues the impaired social behavior in genetic, environmental, and idiopathic mouse models of ASD.

In addition, we sought to identify the mechanism by which a given bacterial strain (*L. reuteri*) regulates a selective behavior or disease state, which represents one of the most important challenges in microbiome research. More specifically, integrating multiple approaches, such as genetics, metagenomics, targeted vagotomies, immunohistochemistry, electrophysiology, and behavior, we began to dissect how *L. reuteri* impacts brain function. At the cellular and molecular levels, we provide new causal evidence that *L. reuteri* modulates social behavior and related changes in synaptic function within the social reward circuits via the oxytocinergic system. Moreover, at the systems level, we found that *L. reuteri* modulates social behavior

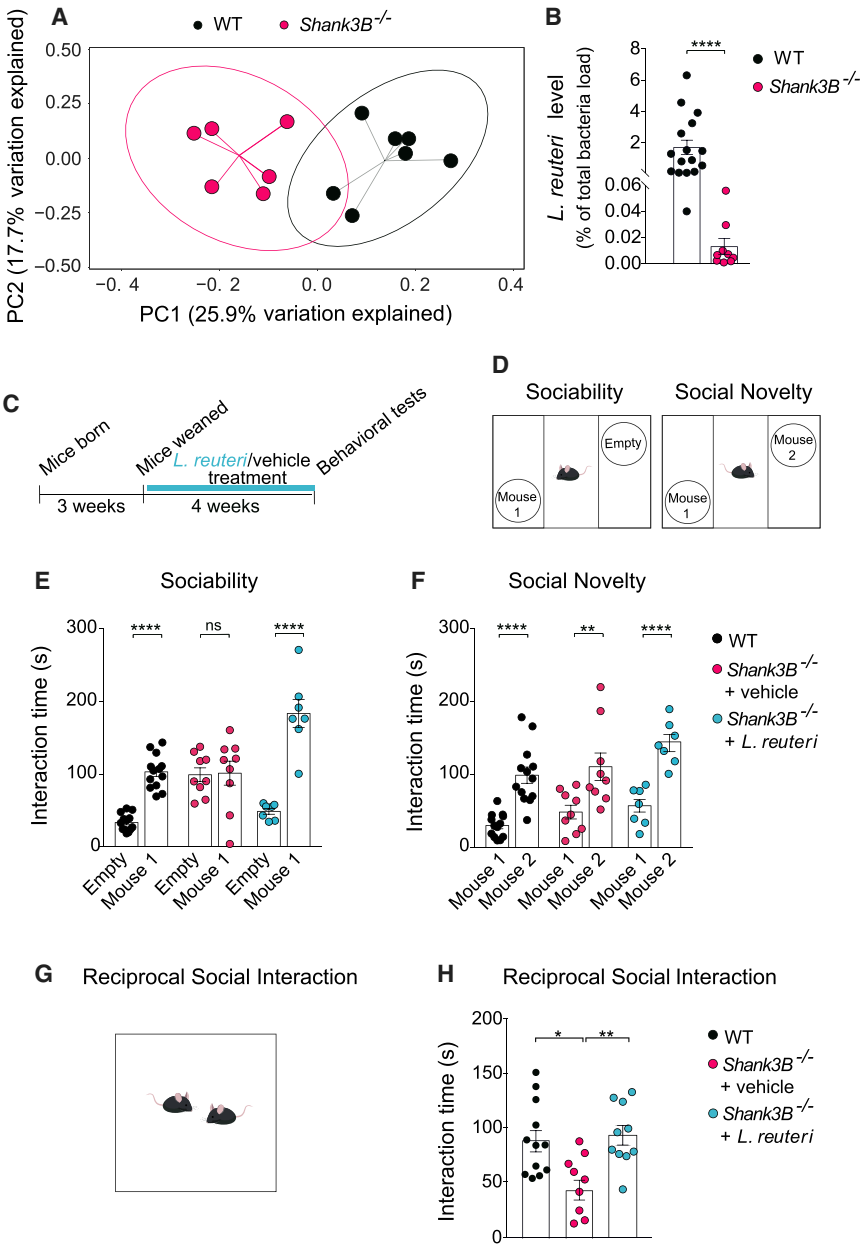


**Figure 1. *Shank3B*$^{-/-}$ Mice Exhibit Changes in Their Microbial Composition, Reduced *L. reuteri* Levels, and Social Deficits that Were Rescued by Treatment with *L. reuteri***

(A) Principal coordinates analysis (PCoA) of unweighted UniFrac distances from the 16S rRNA gene-sequencing dataset shows that *Shank3B*$^{-/-}$ samples clustered separately from those of WT littermates (n = 6–7 per group; $p < 0.01$, $R^2 = 0.225$; 8,024 reads/sample).

(B) qPCR analysis shows lower levels of *L. reuteri* in *Shank3B*$^{-/-}$ mice (as % of total bacteria, n = 9–16 per group; WT versus *Shank3B*$^{-/-}$: Mann-Whitney test, $p < 0.0001$).

(C) Schematic of experimental design.

(D) Schematic of the three-chamber task.

(E and F) In *Shank3B*$^{-/-}$ mice, *L reuteri* rescued social behavior deficits in the three-chamber test (E, Sociability, n = 7–13 per group; WT, $t = 5.68$, $p < 0.0001$; *Shank3B*$^{-/-}$ + vehicle, $t = 0.14$, $p = 0.99$; *Shank3B*$^{-/-}$ + *L. reuteri*, $t = 8.066$, $p < 0.0001$; two-way ANOVA, $F_{2,52} = 17.9$, $p < 0.0001$; F, Social Novelty, n = 7–13 per group; WT, $t = 5.01$, $p < 0.0001$; *Shank3B*$^{-/-}$ + vehicle, $t = 3.75$, $p < 0.01$; *Shank3B*$^{-/-}$ + *L. reuteri*, $t = 4.63$, $p < 0.0001$; two-way ANOVA, $F_{2,52} = 0.52$, $p = 0.59$).

(G) Schematic of the reciprocal social interaction task.

(H) *L. reuteri* rescued reciprocal social interaction deficits in *Shank3B*$^{-/-}$ mice (n = 9–12 pairs per group; WT versus *Shank3B*$^{-/-}$ + vehicle, $t = 3.03$, $p < 0.05$; *Shank3B*$^{-/-}$ + vehicle versus *Shank3B*$^{-/-}$ + *L. reuteri*, $t = 3.20$, $p < 0.01$; WT versus *Shank3B*$^{-/-}$ + *L. reuteri*, $t = 0.32$, $p > 0.99$; one-way ANOVA, $F_{2,28} = 6.3$, $p = 0.0055$). ns, not significant. Plots show mean ± SEM. See also Figures S1–S5 and S15.

independent of other microbes in the gut, and in a vagus nerve-dependent manner. Collectively, our findings provide new mechanistic insight into the gut-brain-axis signaling by which *L. reuteri* influences central nervous system function and selective behaviors.

## RESULTS

### *Shank3B*$^{-/-}$ Mice Show Alterations in the Composition of the Gut Microbiota, and Treatment with *L. reuteri* Rescues Their Social Deficits

Variants in human *SHANK3* lead to Phelan-McDermid syndrome and other non-syndromic ASDs (Jiang and Ehlers, 2013). Mice lacking the Shankβ isoform of the *Shank3* gene (*Shank3B*$^{-/-}$ mice) exhibit ASD-like behaviors, including social deficits (Peça et al., 2011). Given that individuals with ASD often show changes in their gut microbial ecology (Ding et al., 2017; Vuong and Hsiao, 2017), we wondered whether *Shank3B*$^{-/-}$ mice display alteration of their gut microbial composition. To answer this question, we performed 16S ribosomal RNA (rRNA) gene sequencing on fecal samples from *Shank3B*$^{-/-}$ mice and wild-type (WT) littermates, as previously described (Buffington et al., 2016). Bacterial composition, computed based on weighted UniFrac distances (the assessment of community structure by considering abundance of operational taxonomic units, OTUs) or Shannon diversity index, was not significantly altered in *Shank3B*$^{-/-}$ mice compared to WT littermates (Figures S1A–S1D). By contrast, the bacterial diversity measured by unweighted UniFrac analysis, which assesses community structure by considering only the presence or absence of OTUs, revealed a significant difference in the phylogenetic profile of the microbial communities between genotypes (Figure 1A).

It is noteworthy that *Shank3B*$^{-/-}$ mice were obtained from heterozygous (*Shank3B*$^{+/-}$) breeding, as recommended for microbiome studies (Stappenbeck and Virgin, 2016), ruling out potential differences in maternal care and/or early life effects of the gut microbiome. More importantly, we found that the microbiome changes depend on the genotype, but not on cage housing conditions (the so called "cage effect"). For instance, WT mice clustered together regardless of their cage of origin (cage A, B, C, or D). The same is true for *Shank3B*$^{-/-}$ (KO) mice (Figure S2).

Moreover, we found that *Shank3B*$^{-/-}$ mice specifically have lower levels of *L. reuteri* compared to their WT littermates (Figure 1B). Thus, *Shank3B*$^{-/-}$ mice exhibit an altered gut microbial composition, including decreased *L. reuteri* levels in their gut.

Social deficits are one of the most salient features of individuals with ASD (American Psychiatric Association, 2013), and *Shank3B*$^{-/-}$ mice exhibit impaired social behavior (Peça et al., 2011). To examine whether reduced *L. reuteri* levels in the gut of *Shank3B*$^{-/-}$ mice could account for their social behavioral deficits, *Shank3B*$^{-/-}$ mice were treated with either vehicle or *L. reuteri*, added daily in drinking water for 4 weeks (Figure 1C). Social behaviors were first examined in the three-chamber sociability and social novelty tests, as we previously described (Buffington et al., 2016). To test sociability, we compared the time that the experimental mouse spent interacting with either a stranger mouse (Mouse 1) or an empty wired cup (Empty, Figure 1D). As expected, WT mice displayed normal sociability, as reflected by their preferential interaction with the stranger mouse. By contrast, *Shank3B*$^{-/-}$ mice showed no preference for the stranger mouse over the empty cup, indicating impaired sociability (Figure 1E). The social deficits in *Shank3B*$^{-/-}$ mice are not due to alterations in their olfactory ability, since olfaction was not impaired in these mice, as determined by the buried food test (Figure S3A). In addition, we found that, as in WT controls, *Shank3B*$^{-/-}$ mice displayed normal preference for social novelty, as they spent more time interacting with the novel mouse (Mouse 2) than with the familiar one (Mouse 1; Figure 1F). Interestingly, we found that only one cohort of *Shank3B* heterozygous (*Shank3B*$^{+/-}$) mice showed impaired social behavior (Figures S4A, S4C, and S4E). Thus, given the weak social behavior deficits in *Shank3B*$^{+/-}$ mice, we focused on the homozygous knockout line (*Shank3B*$^{-/-}$ mice), which consistently showed an impairment in sociability (Figures S4A, S4C, and S4E).

Remarkably, treatment with *L. reuteri* rescued sociability in *Shank3B*$^{-/-}$ mice. Indeed, the performance of *L. reuteri*-treated *Shank3B*$^{-/-}$ mice was similar to that of WT controls (Figure 1E). To further support these findings, we next assessed reciprocal social interaction (Figure 1G) by measuring the amount of time that stranger, genotype- and treatment-matched mice spent interacting as pairs. *Shank3B*$^{-/-}$ mice interacted significantly less than WT littermates, and treatment with *L. reuteri* reversed the social deficits in the mutant mice (Figure 1H). It is noteworthy that *Shank3B*$^{-/-}$ mice are hypo-active, a condition that was not improved by *L. reuteri* (Figure S5). Thus, treatment with *L. reuteri* selectively reverses the ASD-like social deficits in *Shank3B*$^{-/-}$ mice.

## The VPA Mouse Model of ASD Shows Alterations in the Composition of the Gut Microbiota, and Treatment with *L. reuteri* Rescues Its Social Deficits

Environmental factors may account for a large proportion of the ASD cases (Hallmayer et al., 2011). In mammals, both pre- and post-natal periods are critical developmental windows ultimately influencing behavior during adulthood. During these early developmental periods, environmental factors can change the microbial composition of the host, and affect brain physiology and function via the so-called gut-microbiota-brain axis (Borre et al., 2014; Sharon et al., 2016; Vuong et al., 2017). For instance, among the environmental factors, maternal exposure to different nutrients (e.g., HFD) and/or substances (e.g., valproic acid, VPA) during pregnancy has been associated with ASD (Ornoy, 2009; Sullivan et al., 2014). More specifically, clinical studies have shown that maternal exposure to VPA, a branched short-chain fatty acid used as an antiepileptic drug, is associated with increased risk of ASD incidence in offspring (Christensen et al., 2013; Ornoy, 2009). Accordingly, in rodents, VPA administration during gestation leads to ASD-like behaviors (notably social deficits) in offspring (Kim et al., 2017). Given that the MHFD environmental mouse model of ASD shows social deficits that are mediated by changes in the microbiome (Buffington et al., 2016), we wondered whether the VPA mouse model of ASD is also characterized by alterations in their microbial ecology. Indeed, we found changes in the composition of the microbiota of VPA-treated mice (Figures S6A–S6E), but *L. reuteri* levels were not reduced in these mice (Figure S6F).

Given that (1) VPA alters oxytocin-mediated changes in synaptic transmission (Tyzio et al., 2014), (2) intranasal oxytocin rescues social deficits in VPA-exposed mice (Hara et al., 2017) and other mouse models of ASD (Buffington et al., 2016; Peña-garikano et al., 2015), and (3) *L. reuteri* promotes oxytocin levels (Buffington et al., 2016; Poutahidis et al., 2013), we next wondered whether treatment with *L. reuteri* would improve the social deficits in the offspring from VPA mice. Interestingly, unlike treatment with vehicle, treatment with *L. reuteri* ameliorates the social deficits in VPA mice (Figures S6G and S6H). Taken together, these data demonstrate that, like in the MHFD model, *L. reuteri* also corrects the social deficits in another environmental model of ASD (VPA) with alterations in the gut microbiome.

## BTBR Mice Show Alterations in the Composition of the Gut Microbiota, and Treatment with *L. reuteri* Rescues Their Social Deficits

Several environmental and genetic factors have been identified to be associated with increased incidence of ASD (Hallmayer et al., 2011; Kim and Leventhal, 2015). However, the majority of the ASD cases remain idiopathic. The BTBR T+ Itpr3tf/J (BTBR) inbred mouse line exhibits the core ASD symptoms, including abnormal social behavior (McFarlane et al., 2008; Scattoni et al., 2008). Given that no genetic variants in ASD risk genes have been identified in the BTBR genome (Jones-Davis et al., 2013), this model is considered an idiopathic model of ASD (Meyza and Blanchard, 2017).

While previous studies have shown that BTBR mice harbor a different microbial community in the gut (Coretti et al., 2017;

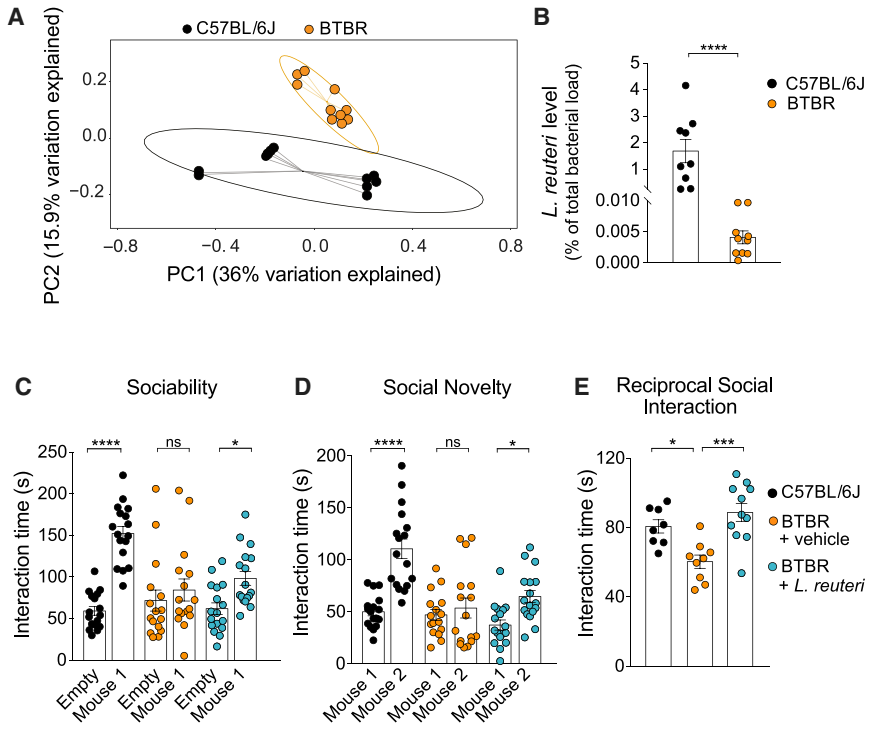


**Figure 2. BTBR Mice Exhibit Changes in Microbial Composition, Reduced *L. reuteri* Levels, and Social Deficits that Were Rescued by Treatment with *L. reuteri***

(A) PCoA of unweighted UniFrac distances from the 16S rRNA gene-sequencing dataset shows that BTBR samples clustered separately from C57BL/6J samples (n = 10–11 per group; $p < 0.01$, $R^2 = 0.164$; 8,024 reads/sample).

(B) qPCR analysis shows lower levels of *L. reuteri* (as % of total bacteria, n = 9–10 per group; C57BL/6J versus BTBR, Mann-Whitney test, $p < 0.0001$) in BTBR mice.

(C–E) In BTBR mice, *L. reuteri* rescued social behavior deficits in the three-chamber test (C, Sociability, n = 16–17 per group; C57BL/6J, $t = 7.033$, $p < 0.0001$; BTBR + vehicle, $t = 0.93$, $p > 0.99$; BTBR + *L. reuteri*: $t = 2.75$, $p < 0.05$; two-way ANOVA, $F_{2,94} = 9.54$, $p < 0.001$; D, Social Novelty, n = 16–17 per group; C57BL/6J, $t = 6.35$, $p < 0.0001$; BTBR + vehicle, $t = 0.67$, $p > 0.99$; BTBR + *L. reuteri*, $t = 2.87$, $p < 0.05$; two-way ANOVA, $F_{2,94} = 7.935$, $p < 0.001$) and the reciprocal social interaction test (E, n = 8–11 pairs per group; C57BL/6J versus BTBR + vehicle, $t = 3.03$, $p < 0.05$; BTBR + vehicle versus BTBR + *L. reuteri*: $t = 4.57$, $p < 0.001$; C57BL/6J versus BTBR + *L. reuteri*, $t = 1.25$, $p = 0.67$; one-way ANOVA, $F_{2,27} = 10.79$, $p < 0.001$). ns, not significant. Plots show mean ± SEM. See also Figures S6, S7, and S15.

Golubeva et al., 2017) and cohousing with C57BL/6J mice has been shown to restore their social deficits (Yang et al., 2011), the nature of the bacterial species which may be causally related to the social behavioral deficits in this ASD model remains unknown. Accordingly, we also found a markedly altered gut microbiome composition in BTBR mice compared to C57BL/6J mice (Figures 2A and S7). Moreover, we found a specific reduction in *L. reuteri* levels in BTBR mice (Figure 2B). Given that both *Shank3B*$^{-/-}$ and BTBR mice exhibit alterations in their gut microbial composition and decreased *L. reuteri* levels and that *L. reuteri* is sufficient to restore the social behavior in *Shank3B*$^{-/-}$ and VPA mice, we next wondered whether this selective microbial intervention would also be effective in BTBR mice. Indeed, treatment with *L. reuteri* improved the social deficits in the three chamber and reciprocal social interaction tasks in the BTBR mice (Figures 2C–2E). Similarly to the *Shank3B*$^{-/-}$ mice, social deficits in BTBR mice were not due to impaired olfaction (see Figure S3B). Taken together, our data show that treatment with *L. reuteri* selectively reverses the ASD-like social deficits in genetic, environmental, and idiopathic models of ASD.

## *L. reuteri* Rescues Social Deficits Independent of Other Gut Microbes

To dissect the mechanism(s) through which *L. reuteri* restores social behavior, we mainly focused on the *Shank3B*$^{-/-}$ model. We first asked whether *L. reuteri* exerts its effects on social behaviors directly, or indirectly by correcting the altered microbial composition of the host. To answer this question, we first analyzed the composition of the gut microbiota in vehicle-treated and *L. reuteri*-treated *Shank3B*$^{-/-}$ mice, as determined by 16S rRNA gene sequencing. We found that treatment with *L. reuteri* did not significantly alter the microbial profile of either *Shank3B*$^{-/-}$ mice (Figure 3A) or BTBR mice (Figure S8). Hence, *L. reuteri* has no significant impact in the overall microbial composition of the host.

To causally demonstrate whether the effects of *L. reuteri* on social behavior are dependent on its interaction with other members of the microbial community, mice raised under sterile conditions (i.e., germ-free [GF] mice) were monocolonized with *L. reuteri* at weaning, and social behavior was tested in 8-week-old mice. As previously described, unlike conventionally colonized mice, GF mice displayed social deficits (Buffington et al., 2016; Desbonnet et al., 2014). Remarkably, monocolonization with *L. reuteri* was sufficient to reverse the social deficits in GF mice (Figures 3B–3D), supporting the notion that *L. reuteri* acts solo, rescuing social behavior in the absence of other members of the community.

## *L. reuteri* Reverses Deficits in Social Behavior via the Vagus Nerve

It is widely accepted that there is a bidirectional gut-microbiota-brain axis, where bacteria initiate signals that are transmitted from the gut to the CNS, either through blood circulation or via the vagus nerve (Borre et al., 2014; Sharon et al., 2016; Vuong et al., 2017). If the integrity of the host's intestinal barrier is damaged and rendered more permeable (so-called "leaky gut"), which occurs when the gut epithelium tight junctions are impaired (Suzuki, 2013), bacteria and/or metabolites produced by bacteria can enter the blood circulation. Indeed, alterations in gut permeability have been described in individuals with

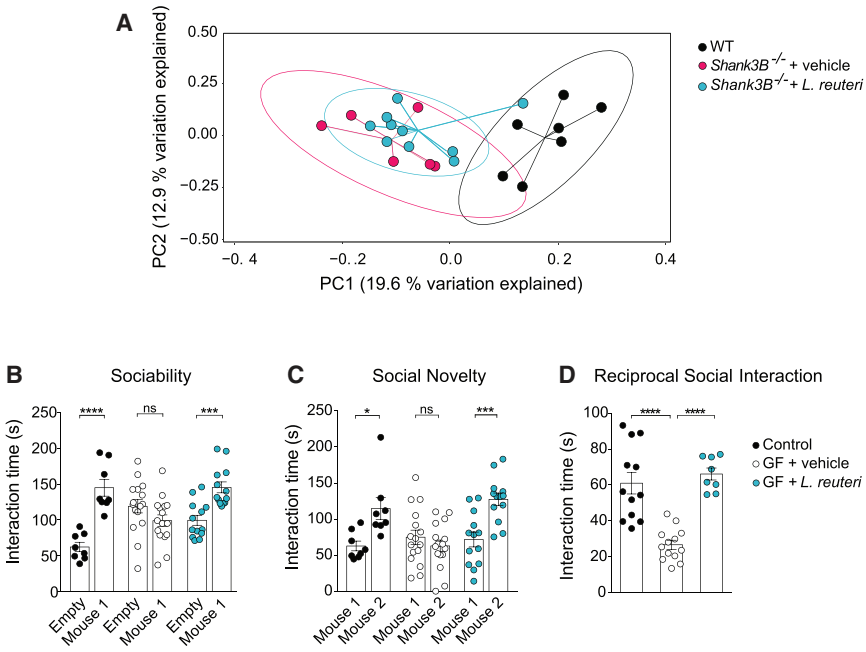


**Figure 3. *L. reuteri* Does Not Change the Microbial Composition of *Shank3B*$^{-/-}$ Mice and Is Sufficient to Rescue Social Deficits in Germ-free Mice**

(A) PCoA of unweighted UniFrac distances from the 16S rRNA gene-sequencing dataset shows that treatment with *L. reuteri* did not significantly alter the clustering of *Shank3B*$^{-/-}$ samples (n = 6–10 per group; $p < 0.001$; $R^2 = 0.215$, 8,024 reads/sample).

(B–D) In GF mice, *L. reuteri* reversed social behavior deficits in the three-chamber test (B, Sociability, n = 8–16 per group; Controls, $t = 5.44$, $p < 0.0001$; GF + vehicle, $t = 1.87$, $p = 0.20$; GF + *L. reuteri*, $t = 3.85$, $p < 0.001$; two-way ANOVA, $F_{2,68} = 16.64$, $p < 0.0001$; C, Social Novelty, n = 8–16 per group; Controls, $t = 3.00$, $p < 0.05$; GF + vehicle, $t = 1.28$, $p = 0.61$; GF + *L. reuteri*, $t = 4.10$, $p < 0.001$; two-way ANOVA, $F_{2,68} = 7.63$, $p = 0.0010$) and the reciprocal social interaction test (D, n = 8–13 pairs per group; Controls versus GF + vehicle, $t = 5.89$, $p < 0.0001$; Controls versus GF + *L. reuteri*, $t = 0.77$, $p > 0.99$; GF + vehicle versus GF + *L. reuteri*, $t = 6.03$, $p < 0.0001$; one-way ANOVA, $F_{2,30} = 24.87$, $p < 0.0001$). ns, not significant. Plots show mean ± SEM. See also Figure S8.

ASD (Julio-Pieper et al., 2014; Mayer et al., 2014). Thus, we first tested whether *Shank3B*$^{-/-}$ mice show increased intestinal permeability. To this end, we administered fluorescein isothiocyanate-dextran (FITC-dextran) by oral gavage and measured its concentration in the serum, as described (Gupta and Nebreda, 2014). If the intestinal barrier is compromised in *Shank3B*$^{-/-}$ mice, we would expect increased FITC-dextran in the serum of these mice. As expected, our positive control mice administrated with dextran sodium sulfate (DSS), a chemical which induces colitis, exhibited a leaky gut, as determined by increased FITC-dextran in their serum (Figure 4A). By contrast, compared to control littermates, *Shank3B*$^{-/-}$ mice showed no changes in gut permeability (Figure 4A). Accordingly, the expression of key tight junction proteins was not altered in *Shank3B*$^{-/-}$ mice, as determined by reverse transcription followed by quantitative PCR (RT-qPCR) (Figure 4B). Thus, *Shank3B*$^{-/-}$ mice did not show major alterations in gut permeability.

We then investigated whether, for *L. reuteri*, the vagus nerve could serve as a channel of communication between the gut and the brain. Previous studies have shown that the vagus nerve is activated in response to specific bacteria (Perez-Burgos et al., 2014; Perez-Burgos et al., 2013) and that the *Lactobacillus* species *L. rhamnosus* reduces anxiety-related behavior in a vagus-dependent manner (Bravo et al., 2011). To determine whether the vagus nerve is required for *L. reuteri* to reverse the social deficits in *Shank3B*$^{-/-}$ mice, we performed bilateral subdiaphragmatic vagotomy in these mice (Figure 4C). Control mice (sham-operated mice) underwent the same surgical procedures, except that the vagal branches were not transected. If the vagus nerve is required for the relevant gut-microbiota-brain communication, *L. reuteri* should fail to rescue the social deficits in vagotomized *Shank3B*$^{-/-}$ mice. Consistent with this hypothesis, we found that *L. reuteri* rescued social behaviors in sham-operated, but not in vagotomized *Shank3B*$^{-/-}$ mice (Figures 4D and 4F). Results from several control experiments underscore the specificity of the vagotomy to the effects of *L. reuteri* on social behavior. First, the vagotomy was complete, as determined by a food intake analysis based on the satiating effect of cholecystokinin-octapeptide (CCK-8), which depends on the vagus nerve (Joyner et al., 1993; Figure S9A). Second, social behavior was similar in WT-sham and WT-vagotomized mice (Figures S9B–S9D). Moreover, preference for social novelty, which is not impaired in *Shank3B*$^{-/-}$ mice, was not affected by the vagotomy (Figure 4E), indicating that the vagotomy itself had no effect on social behavior. Third, vagotomy did not affect motor behavior (Figures S9E–S9H). Finally, intranasal oxytocin-treatment, which bypasses the gut-microbiota-brain communication channel, restored social behaviors in vagotomized *Shank3B*$^{-/-}$ mice (see Figures 6D and 6E), demonstrating that the vagotomy procedure did not prevent the animals' ability to perform the social task. Thus, *L. reuteri* reversed the social deficits in *Shank3B*$^{-/-}$ mice in a vagus nerve-dependent manner.

## Oxytocin Rescues Social Behavioral Deficits in Genetic, Environmental, and Idiopathic Models of ASD

Oxytocin modulates numerous aspects of social behaviors and is implicated in ASD (Donaldson and Young, 2008; LoParo and Waldman, 2015). Treatment with oxytocin reverses social deficits in several mouse models of ASD (Buffington et al., 2016; Hara et al., 2017; Harony-Nicolas et al., 2017; Peñagarikano et al., 2015). Additionally, it is known that vagal nerve fibers project to the PVN (Sabatier et al., 2013; Uvnäs-Moberg et al., 2015), a brain region where oxytocin is produced, and that neuronal activity in the PVN induced by bacterial colonization is blocked by subdiaphragmatic vagotomy (Wang et al., 2002). Finally,

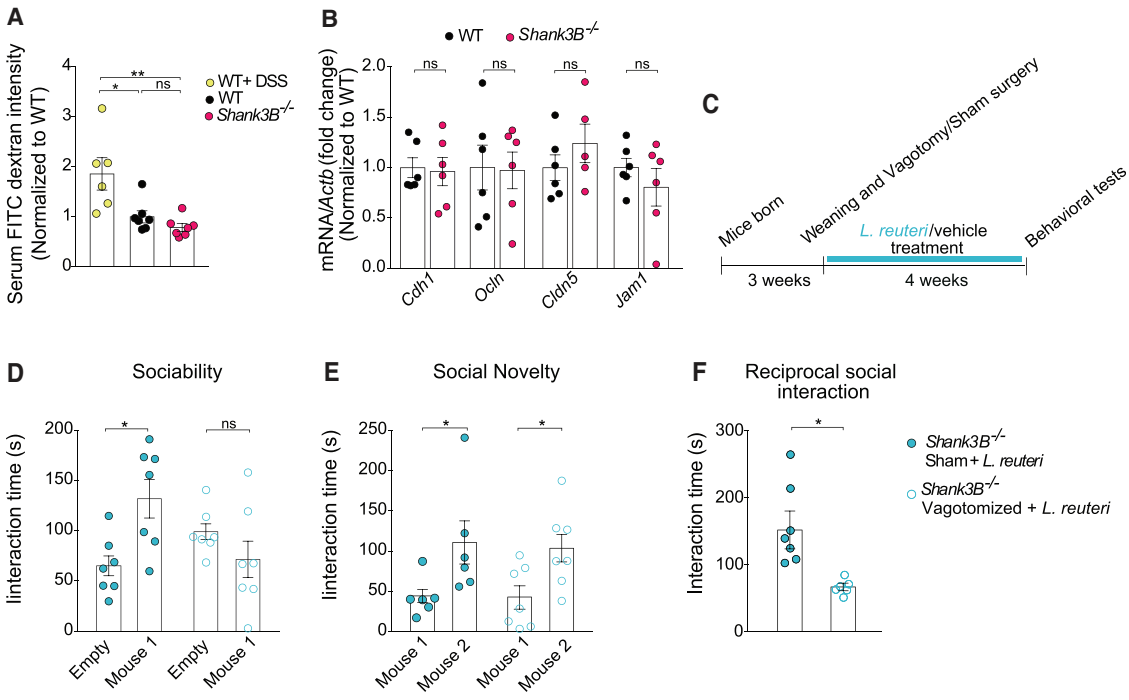


**Figure 4. *Shank3B*$^{-/-}$ Mice Show No Alterations in Intestinal Permeability, and *L. reuteri* Fails to Improve Social Behavior in Vagotomized *Shank3B*$^{-/-}$ Mice**

(A) Intestinal permeability assay by FITC intensity shows no difference between *Shank3B*$^{-/-}$ mice and WT littermates (n = 6–7 per group; WT + DSS versus WT, $t = 3.17$, $p < 0.05$; WT+ DSS versus *Shank3B*$^{-/-}$, $t = 3.95$, $p < 0.01$; WT versus *Shank3B*$^{-/-}$, $t = 0.81$, $p > 0.99$; one-way ANOVA, $F_{2,17} = 8.6$, $p = 0.0026$).

(B) Expression of gut tight junction components was unaltered in *Shank3B*$^{-/-}$ mice, as determined by RT-qPCR (n = 5–6 per group; WT versus *Shank3B*$^{-/-}$, *Cdh1* $t = 0.17$, $p > 0.99$; *Ocln* $t = 0.13$, $p > 0.99$, *Cldn5* $t = 1.03$, $p > 0.99$; *Jam1* $t = 0.87$, $p > 0.99$; one-way ANOVA, $F_{3,39} = 0.62$, $p = 0.60$).

(C) Schematic of the vagotomy experimental design.

(D–F) In vagotomized *Shank3B*$^{-/-}$ mice, *L. reuteri* failed to reverse social behavior deficits in the three-chamber test (D, Sociability, n = 7 per group; *Shank3B*$^{-/-}$ Sham + *L. reuteri*, $t = 3.22$, $p < 0.05$; *Shank3B*$^{-/-}$ Vagotomized + *L. reuteri*, $t = 1.33$, $p = 0.35$; two-way ANOVA, $F_{1,24} = 10,4$, $p = 0.003$; E, Social Novelty, n = 7 per group; *Shank3B*$^{-/-}$ Sham + *L. reuteri*, $t = 2.56$, $p < 0.05$; *Shank3B*$^{-/-}$ Vagotomized + *L. reuteri*: $t = 2.60$, $p < 0.05$; two-way ANOVA, $F_{1,22} = 0.028$, $p = 0.86$) and reciprocal social interaction test (F, n = 6–7 pairs per group; *Shank3B*$^{-/-}$ Sham + *L. reuteri* versus *Shank3B*$^{-/-}$ Vagotomized + *L. reuteri*, Mann-Whitney Test $p < 0.01$). DSS, dextran sodium sulfate; ns, not significant. Plots show mean ± SEM. See also Figure S9.

stimulation of the vagus nerve can promote oxytocin release (Stock and Uvnäs-Moberg, 1988).

We and others have shown that *L. reuteri* increases oxytocin levels (Buffington et al., 2016; Poutahidis et al., 2013). Interestingly, we found a reduction in oxytocin-positive neurons in the PVN (Figure 5A) of *Shank3B*$^{-/-}$ mice compared to WT littermates (Figures 5B and 5C). The number and fluorescence intensity of NeuN-positive neurons did not change in the PVN of *Shank3B*$^{-/-}$ mice (Figures 5B, 5D, and 5F), indicating that the decrease in oxytocin-positive neurons in *Shank3B*$^{-/-}$ was not due to a decrease in the total number of neurons. As expected, *L. reuteri* treatment increased both the number and fluorescence intensity of oxytocin-positive neurons in *Shank3B*$^{-/-}$ mice (Figures 5B, 5C, and 5E).

Given that *L. reuteri* treatment promotes oxytocin immunoreactivity in the PVN of *Shank3B*$^{-/-}$ mice and rescues their social deficits, we hypothesized that oxytocin administration would also reverse the social deficits in *Shank3B*$^{-/-}$ mice. As predicted, intranasal oxytocin (Figure 6A) reversed the social deficits in *Shank3B*$^{-/-}$ mice (Figures 6B, 6C, and S10A). Moreover, oxytocin improved the social behaviors that are deficient in VPA (Figures S11A and S11B), BTBR mice (Figures S11C–S11E), and partially in GF mice (Figures S11F–S11H), all models in which *L. reuteri* effectively rescues their social deficits. Interestingly, like *L. reuteri* treatment, oxytocin had no effect on the hypo-activity behavior in the *Shank3B*$^{-/-}$ mice (Figures S10B and S10C). Together, these data suggest that oxytocinergic signaling is involved in the mechanism of action by which *L. reuteri* selectively restores social behavior in several ASD mouse models.

## *L. reuteri* Restores Social Interaction-Induced Synaptic Potentiation in the Ventral Tegmental Area of *Shank3B*$^{-/-}$ Mice, but Not in Mice Lacking the Oxytocin Receptor in Dopaminergic Neurons

Brain regions responding to naturally rewarding stimuli, including the ventral tegmental area (VTA) and the nucleus accumbens (NAc), are crucially involved in social behaviors (Dölen et al., 2013; Gunaydin et al., 2014; Huang and Hessler, 2008). In addition, oxytocin-expressing neurons in the PVN project to the VTA (Melis et al., 2007). Oxytocin activates VTA neurons in both mice and humans, influencing the processing of socially relevant cues

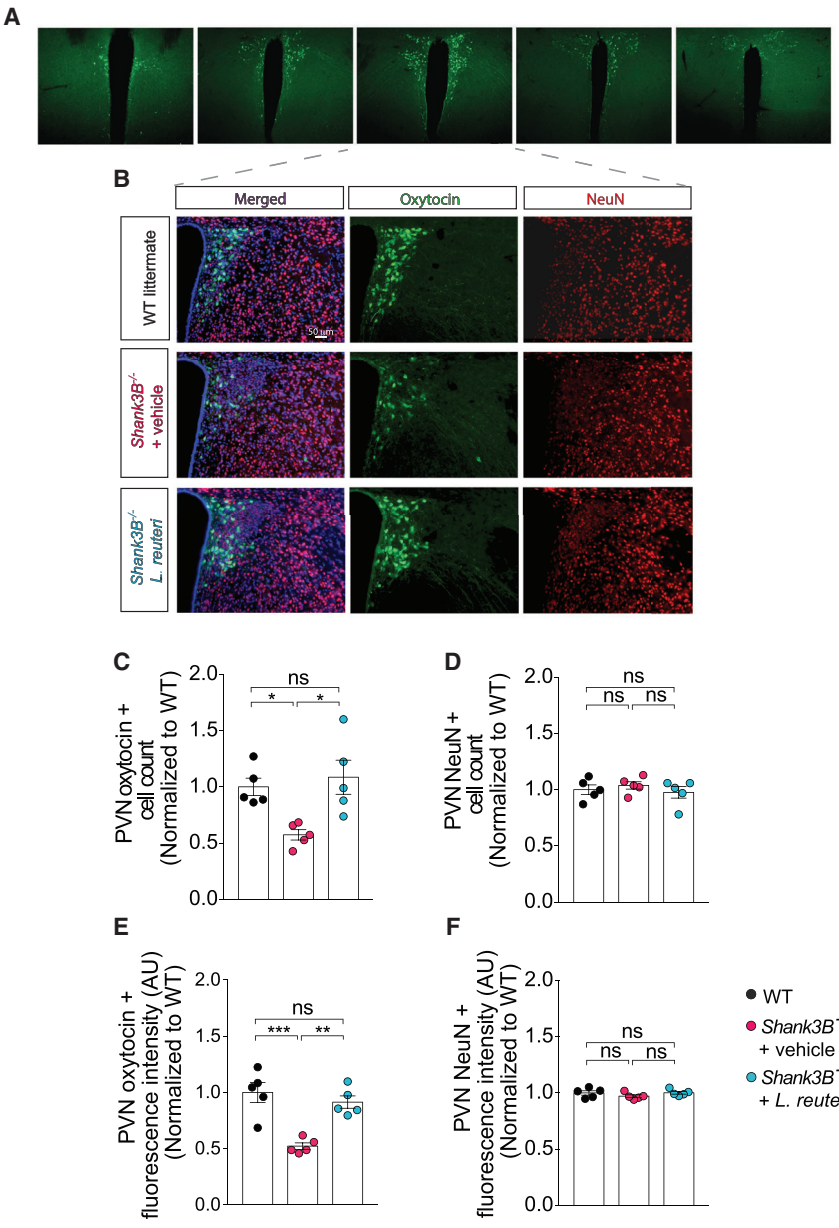


**Figure 5. *L. reuteri* Treatment Corrects Oxytocin Levels in the PVN of the Hypothalamus of *Shank3B*$^{-/-}$ Mice**

(A) Representative images of oxytocin-positive neurons at different antero-posterior levels of the PVN of control mice.

(B) Oxytocin immunoreactivity in the PVN of WT and *Shank3B*$^{-/-}$ mice treated with either vehicle or *L. reuteri*.

(C–F) Oxytocin-positive cell number (C, n = 5 mice per group; WT versus *Shank3B*$^{-/-}$ + vehicle, $t$ = 2.96, $p < 0.05$; Shank*3B*$^{-/-}$ + vehicle versus *Shank3B*$^{-/-}$ + *L. reuteri*: $t$ = 3.64, $p < 0,05$; WT versus *Shank3B*$^{-/-}$ + *L. reuteri*, $t$ = 0.59, $p > 0.99$; one-way ANOVA, $F_{2,12} = 7.28$, $p = 0.0085$) and oxytocin immunofluorescence intensity (E, n = 5 mice per group; WT versus *Shank3B*$^{-/-}$ + vehicle, $t$ = 5.38, $p < 0.001$; *Shank3B*$^{-/-}$ + vehicle versus *Shank3B*$^{-/-}$ + *L. reuteri*, $t$ = 4.41, $p < 0.01$; WT versus *Shank3B*$^{-/-}$ + *L. reuteri*, $t$ = 0.96, $p$ = 0.0025; one-way ANOVA, $F_{2,12} = 16.49$, $p = 0.0004$) are restored after *L. reuteri* treatment. The number (D, n = 5 mice per group, WT versus *Shank3B*$^{-/-}$ + vehicle, $t$ = 0.62, $p > 0.99$; *Shank3B*$^{-/-}$ + vehicle versus *Shank3B*$^{-/-}$ + *L. reuteri*, $t$ = 1.01, $p$ = 0.99, WT versus *Shank3B*$^{-/-}$ + *L. reuteri*, $t$ = 0.38, $p > 0.99$; one-way ANOVA, $F_{2.12} = 0.52$, $p = 0.60$) and the fluorescence intensity (F, n = 5 mice per group, WT versus *Shank3B*$^{-/-}$ + vehicle, $t = 1.34$, $p = 0.61$; *Shank3B*$^{-/-}$ + vehicle versus *Shank3B*$^{-/-}$ + *L. reuteri*, $t = 1.42$, $p = 0.54$; WT versus *Shank3B*$^{-/-}$ + *L. reuteri*, $t$ = 0.07, $p > 0.99$; one-way ANOVA, $F_{2,12} = 1.27$, $p = 0.31$) of NeuN-positive cells did not change between the groups. ns, not significant. Plots show mean ± SEM.

(Gregory et al., 2015; Groppe et al., 2013; Hung et al., 2017; Tang et al., 2014; Xiao et al., 2017), and oxytocin receptor blockade in the VTA prevents social attachment in rodents (Pedersen et al., 1994). Moreover, optogenetic stimulation of VTA-NAc projections promotes social interaction (Gunaydin et al., 2014). Social interaction, which can be particularly rewarding, triggers synaptic potentiation in VTA dopamine (DA) neurons of both birds (Huang and Hessler, 2008) and mice (Buffington et al., 2016). Since the oxytocinergic system is impaired in *Shank3B*$^{-/-}$ mice, we hypothesized that social interaction-induced VTA plasticity would be deficient in these mice. To test this hypothesis, we recorded direct social interaction-evoked long-term potentiation (LTP) in VTA DA neurons (Figures 7A and S12A–S12C) by measuring the ratio of alpha-amino-3-hydroxy-5-methyl-4-isoxazolepropionic acid receptor (AMPAR) to N-methyl-d-aspartate receptor (NMDAR) currents, as we previously described (Buffington et al., 2016).

As we recently reported (Buffington et al., 2016), reciprocal social interaction increased the AMPAR/NMDAR in VTA DA neurons from control mice (Figure 7B). By contrast, the same procedure failed to induce synaptic potentiation in *Shank3B*$^{-/-}$ mice (Figure 7B). The inability to induce social interaction-induced synaptic potentiation in *Shank3B*$^{-/-}$ VTA DA neurons was not due to changes in baseline activity or to the failure to respond to any stimuli. In fact, baseline AMPAR/NMDAR ratios were similar in *Shank3B*$^{-/-}$ mice and WT littermates (Figure 7B), and a single injection of cocaine, which has been shown to increase the AMPAR/NMDAR ratio in VTA DA neurons (Huang et al., 2016; Ungless et al., 2001; Figure S12D), evoked LTP in VTA DA neurons of *Shank3B*$^{-/-}$ mice (Figure 7B). Thus, the synaptic potentiation associated specifically with social reward is impaired in *Shank3B*$^{-/-}$ mice. More importantly, we found that *L. reuteri* rescues the deficits in social interaction-induced VTA plasticity in *Shank3B*$^{-/-}$ mice (Figure 7B). Consistent with the notion that the effect of *L. reuteri* on social behavior is mediated by oxytocin,

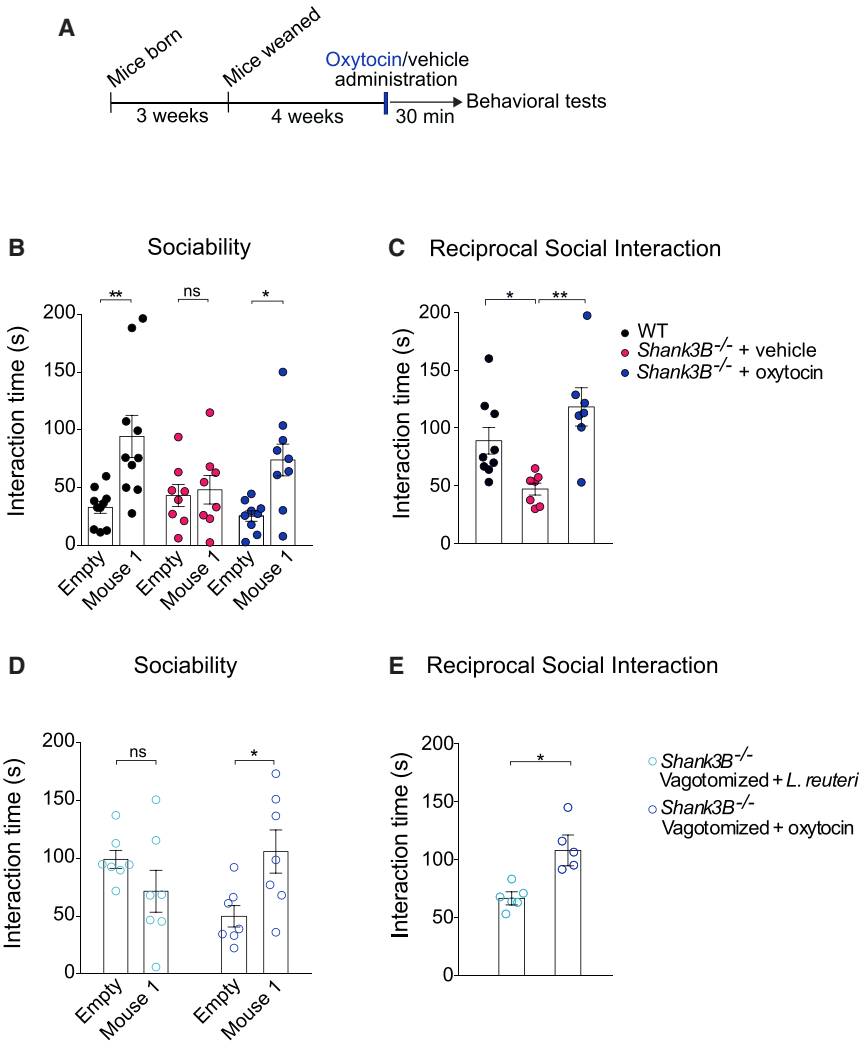


**Figure 6. Oxytocin Administration Rescues Social Deficits in Both *Shank3B*$^{-/-}$ and *Shank3B*$^{-/-}$ Vagotomized Mice**

(A) Schematic of experimental design.

(B and C) In *Shank3B*$^{-/-}$ mice, oxytocin improved social behavior deficits in the three-chamber test (B, Sociability, n = 8–10 per group; WT, $t = 3.84$, $p < 0.01$; *Shank3B*$^{-/-}$ + vehicle, $t = 0.28$, $p > 0.99$; *Shank3B*$^{-/-}$ + oxytocin, $t = 2.88$, $p < 0.05$; two-way ANOVA, $F_{2,48} = 2.94$, $p = 0.06$) and reciprocal social interaction test (C, n = 7–9 pairs per group; WT versus *Shank3B*$^{-/-}$ + vehicle, $t = 2.70$, $p < 0.05$; *Shank3B*$^{-/-}$ + vehicle versus *Shank3B*$^{-/-}$ + oxytocin, $t = 4.02$, $p < 0.01$; WT versus *Shank3B*$^{-/-}$ + oxytocin, $t = 1.45$, $p = 0.49$; one-way ANOVA, $F_{2,19} = 0.0025$).

(D and E) In *Shank3B*$^{-/-}$ vagotomized mice, oxytocin also improved social behavior deficits in the three-chamber test (D, Sociability, n = 7 per group; *Shank3B*$^{-/-}$ Vagotomized + *L. reuteri*, $t = 1.35$, $p = 0.33$; *Shank3B*$^{-/-}$ Vagotomized + oxytocin, $t = 2.76$, $p < 0.05$, two-way ANOVA, $F_{1,24} = 8.46$, $p = 0.0077$) and reciprocal social interaction test (E, n = 5–6 pairs per group; *Shank3B*$^{-/-}$ Vagotomized + *L. reuteri* versus *Shank3B*$^{-/-}$ Vagotomized + oxytocin, Mann-Whitney Test, $p < 0.05$). ns, not significant. Plots show mean ± SEM. See also Figures S10 and S11.

intranasal oxytocin administration also rescued the impaired LTP in VTA DA neurons from *Shank3B*$^{-/-}$ mice (Figure 7B). Hence, social interaction-induced synaptic plasticity is impaired in *Shank3B*$^{-/-}$ mice but restored by treatment with *L. reuteri* or oxytocin.

Because PVN-VTA oxytocinergic projections are crucially involved in social behaviors (Hung et al., 2017; Xiao et al., 2017) and that *L. reuteri* and oxytocin restore social interaction-induced plasticity in VTA DA neurons of ASD models (Buffington et al., 2016; Figure 7B), we wondered whether the effect of *L. reuteri* on social behavior and related changes in social-induced plasticity in the VTA depends on oxytocin signaling. To answer this question, we conditionally deleted oxytocin receptors (*Oxtr*) in DA neurons (see STAR Methods). Deletion of *Oxtr* in DA neurons in DA-*Oxtr*$^{-/-}$ mice had no impact on the levels of *L. reuteri* in the gut (Figure S13). However, compared to control mice, we found that mice lacking *Oxtr* in DA neurons (DA-*Oxtr*$^{-/-}$) were socially impaired (Figure 7C), consistent with a recent report (Hung et al., 2017).

Strikingly, treatment with either *L. reuteri* or oxytocin failed to rescue the deficits in social behaviors (Figure 7C) and related changes in VTA DA synaptic function in DA-*Oxtr*$^{-/-}$ mice (Figure 7D). By contrast, cocaine was able to induce LTP in VTA DA neurons of DA-*Oxtr*$^{-/-}$ mice (Figure 7D), indicating that oxytocin signaling is selectively required for social interaction-induced synaptic plasticity in the reward circuitry. Consistently, administration of the selective oxytocin receptor antagonist L-371,257 to *Shank3B*$^{-/-}$ mice prevented the prosocial effects associated with *L. reuteri* treatment (Figure S14). Collectively, these data show that *L. reuteri* treatment promotes social behaviors and social interaction-mediated synaptic potentiation in an oxytocin-dependent manner.

## DISCUSSION

Traditionally, when we think about the etiology and symptomatology of ASD, we think about the brain. However, recent discoveries that gut microbes could modulate brain function and behavior have added a whole new dimension to this classic view. A large body of preclinical literature supports the notion of a bidirectional communication system linking the gut and the brain, known as the gut-microbiota-brain axis (Borre et al., 2014; Sharon et al., 2016; Vuong et al., 2017). Foundational studies have shown that GF mice or mice treated with a broad spectrum of antibiotics show behavioral abnormalities, including endophenotypes associated with ASD (Arentsen et al., 2015; Bercik et al., 2011a; Desbonnet et al., 2014; Diaz Heijtz et al., 2011; Leclercq et al., 2017; Neufeld et al., 2011).

While most of the focus in the ASD field has been on either genetic or environmental factors associated with the disorder, the gut microbiome lies at the interface between the host and its environment. Moreover, GI symptoms and changes in gut microbial composition are common in ASD individuals (Vuong and Hsiao, 2017). Indeed, while some patients with ASD present a decreased Bacteroidetes/Firmicutes ratio (Strati et al., 2017; Tomova et al., 2015), others show the opposite result (De Angelis et al., 2013; Zhang et al., 2018). We found that *Shank3B*$^{-/-}$ mice show no significant difference in abundance of the two phyla, but the BTBR and VPA models show an increased Bacteroidetes/Firmicutes ratio compared to control mice (Figure S15). Hence, like in humans, changes in the Bacteroidetes/Firmicutes ratio may not be a reliable microbial signature associated with ASD-like behaviors, at least in the ASD mouse models studied here. More importantly, experiments in mouse models have shown that gut microbes can modulate endophenotypes traditionally associated with brain-centered disorders, including ASD (Buffington et al., 2016; Hsiao et al., 2013). Regardless of the initial insult triggering the disorder (genetic or environmental) and the extent of the alterations to the intestinal microbial communities, we found that *L. reuteri* reverses social deficits in genetic, environmental, and idiopathic models of ASD. Thus, our data (in mice) support the idea that microbial therapies could ameliorate specific endophenotypes associated with ASD. More importantly, while most of the studies in the microbiome field so far have been correlational in nature, where the composition of the microbiota is associated to a particular behavioral or disease state, we began to mechanistically dissect how a particular microbe in the gut impacts brain function and behavior. Our results showing that *L. reuteri* is able to reverse the social deficits in different mouse models of ASD hold promise for novel therapies in human patients. However, the gut-microbiota-brain axis is an emerging field, and to ensure the success of microbial-based therapies for neurological disorders, we believe that first it would be important to establish a set of defined and objective criteria for transitioning into human clinical trials. We discuss some of these criteria below:

First, it would be important that the bacterial strain(s) restores the behavioral deficits of interest (e.g., social deficits) in multiple models of a disease, demonstrating the robustness of the microbial intervention. Specifically, we have shown that *L. reuteri* rescues social deficits in several mouse models of ASD, including a genetic model (*Shank3B*$^{-/-}$), three environmental models (VPA, GF, and MHFD; Buffington et al., 2016), and an idiopathic model (BTBR) of ASD (Figures 1, 2, 3, and S6). Future experiments to assess whether *L. reuteri* is also effective in non-mouse models of ASD, such as rats (Harony-Nicolas et al., 2017) or even non-human primates (Zhao et al., 2017), would provide an even stronger rationale for moving toward developing therapies for humans. For instance, studying the effect of *L. reuteri* in pigs would be revealing, since their GI tract is more similar to that of humans (Zhang et al., 2013). However, to our knowledge, pig models with social deficits are not currently available.

Second, it will be of great significance to determine whether the effect of the candidate microbe(s) is direct or indirect—that is, whether the microbe itself is driving the effect or instead modulating the abundance and/or function of other members of the microbial community, which in turn affect behavior. If the latter case, it would be key to define which member(s) of the community is the main player(s). This may ultimately determine whether the therapy will be based on only one microbe (monotherapy) or a combination of bacteria (probiotic cocktail; Olson et al., 2018). Surprisingly, we found that *L. reuteri* alone is sufficient to reverse the social behavioral deficits in GF mice, demonstrating that its effect on social behavior does not depend on other members of the microbial community (Figure 3).

Third, there should be a minimal understanding of the mechanism through which the gut microbe of interest modulates behavior. In this regard, we found that the *L. reuteri*-mediated rescue of social behavior depends on oxytocinergic and dopaminergic reward systems. We and others have previously provided correlational evidence that *L. reuteri* increases oxytocin levels (Buffington et al., 2016; Poutahidis et al., 2013), but causal evidence linking *L. reuteri* and oxytocin signaling during social behavior was missing. Here, we show that *L. reuteri* reverses the social deficits in several mouse models of ASD (Figures 1E–1H, 2C–2E, 3B–3D, and S6G), but it fails to do so in mice lacking oxytocin receptor specifically in dopaminergic neurons (DA-*Oxtr*$^{-/-}$ mice, Figure 7C). Moreover, in *Shank3B*$^{-/-}$ mice in which oxytocin receptors were pharmacologically blocked, treatment with *L. reuteri* was not longer able to reverse the social deficits in these mice (see Figure S14). Accordingly, like *L. reuteri*, oxytocin reverses the social deficits in all of the other ASD mouse models tested (MHFD, VPA, GF, BTBR, and *Shank3B*$^{-/-}$ mice; see Figures 6 and S11 and Buffington et al., 2016), but not in DA-*Oxtr*$^{-/-}$ mice (Figure 7C). Thus, our genetic and pharmacological results support the concept that the effect of *L. reuteri* on social behavior depends on the oxytocinergic systems.

In addition, we have previously found that social interaction-induced LTP in VTA DA neurons was impaired in MHFD mice and that *L. reuteri* reverses these long-lasting synaptic changes that likely underlie the social deficits (Buffington et al., 2016). However, it was not clear whether this form of plasticity was also impaired in genetic models of ASD. Here we found that, like the environmental MHFD model, genetic models of ASD (*Shank3B*$^{-/-}$ and DA-*Oxtr*$^{-/-}$) exhibit impaired social interaction-induced VTA plasticity and social behavior (Figures 1 and 7), indicating that there may be a convergent cellular and synaptic mechanism underlying the neuropathology associated with ASD. More importantly, treatment with both *L. reuteri* and oxytocin reverses the social interaction-induced LTP in VTA DA neurons from *Shank3B*$^{-/-}$ mice, but it fails to do so in DA-*Oxtr*$^{-/-}$ mice (Figure 7D), consistent with the idea that *L. reuteri*-mediated increase in oxytocin enhances the salience and rewarding value of social stimuli. Accordingly, the release of oxytocin from PVN neurons onto VTA DA neurons increases excitability during social interaction (Hung et al., 2017). Taken together, these data support the notion that social behavior (and its mechanisms) can be also studied at the cellular level by measuring changes in synaptic plasticity in VTA dopaminergic neurons upon social interaction.

Moreover, our new results identified the main communication channel between the gut and the brain through which *L. reuteri* improves social behaviors in mouse models of ASD (Figures 4D–4F). It has been previously shown that microbes could

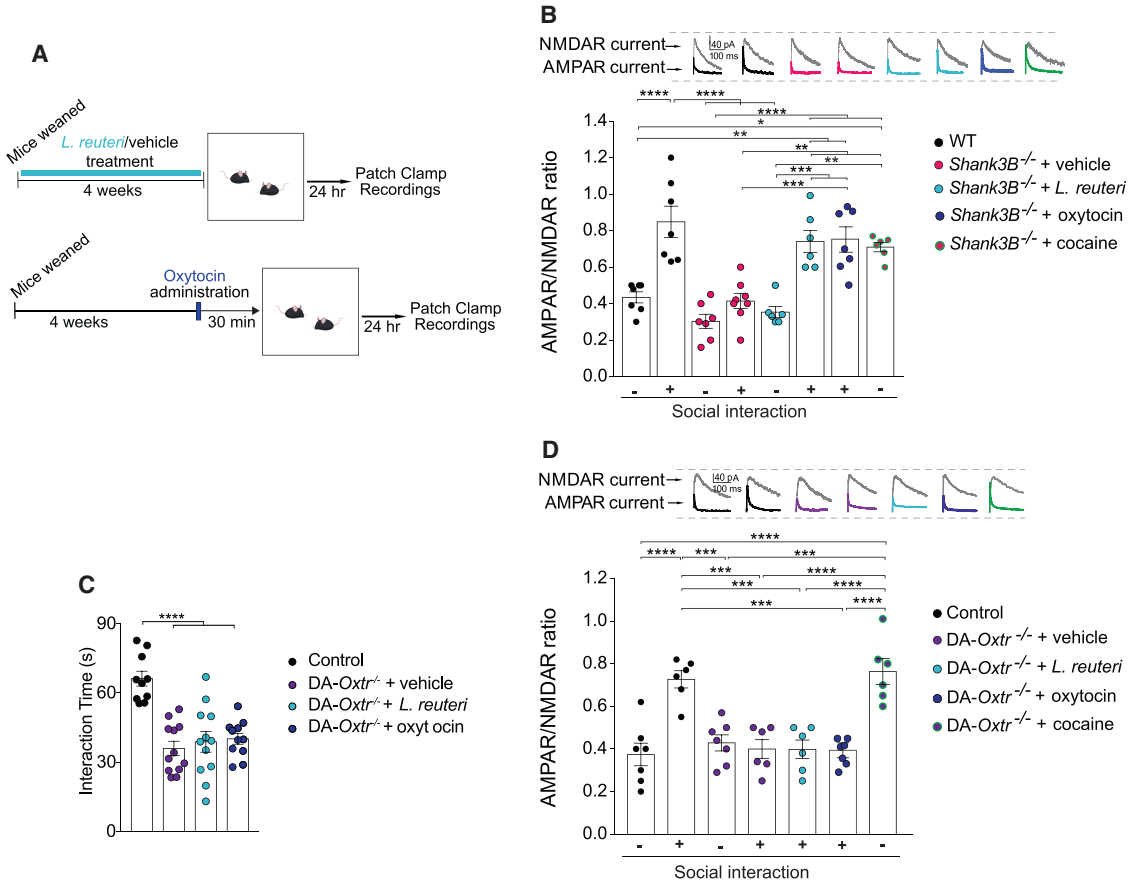


**Figure 7. *L. reuteri* Rescues the Impaired Social Interaction-Induced Synaptic Plasticity in VTA DA Neurons of *Shank3B*$^{-/-}$ Mice, but Not in Mice Lacking Oxytocin Receptors**

(A) Schematic of electrophysiology experiments.

(B) AMPAR/NMDAR ratio in lateral VTA DA neurons recorded at baseline and 24 hr after reciprocal social interaction (n = 6–8; WT baseline versus *Shank3B*$^{-/-}$ + vehicle baseline, $t = 1.81$, $p > 0.99$; WT baseline versus WT social interaction, $t = 5.70$, $p < 0.0001$; WT baseline versus *Shank3B*$^{-/-}$ + vehicle social interaction, $t = 0.29$, $p > 0.99$; WT baseline versus *Shank3B*$^{-/-}$ + *L. reuteri*, $t = 1.07$, $p > 0.99$; WT baseline versus *Shank3B*$^{-/-}$ + *L. reuteri* social interaction, $t = 4.04$, $p < 0.01$; WT baseline versus *Shank3B*$^{-/-}$ + cocaine, $t = 3.64$, $p < 0.05$; WT baseline versus *Shank3B*$^{-/-}$ + oxytocin social interaction, $t = 4.29$, $p < 0.01$; *Shank3B*$^{-/-}$ baseline + vehicle versus WT social interaction, $t = 7.51$, $p < 0.0001$; *Shank3B*$^{-/-}$ + vehicle baseline versus *Shank3B*$^{-/-}$ + vehicle social interaction, $t = 1.58$, $p > 0.99$; *Shank3B*$^{-/-}$ + vehicle baseline versus *Shank3B*$^{-/-}$ + *L. reuteri*, $t = 0.66$, $p > 0.99$, *Shank3B*$^{-/-}$ + vehicle baseline versus *Shank3B*$^{-/-}$ + *L. reuteri* social interaction, $t = 5.78$, $p < 0.0001$; *Shank3B*$^{-/-}$ + vehicle baseline versus *Shank3B*$^{-/-}$ + cocaine, $t = 5.38$, $p < 0.0001$; *Shank3B*$^{-/-}$ + vehicle baseline versus *Shank3B*$^{-/-}$ + oxytocin social interaction $t = 6.1$, $p < 0.0001$; WT social interaction versus *Shank3B*$^{-/-}$ + vehicle social interaction, $t = 6.18$, $p < 0.0001$; WT social interaction versus *Shank3B*$^{-/-}$ + *L. reuteri*, $t = 6.55$, $p < 0.0001$; WT social interaction versus *Shank3B*$^{-/-}$ + *L. reuteri* social interaction, $t = 1.43$, $p > 0.99$; WT social interaction versus *Shank3B*$^{-/-}$ + cocaine, $t = 1.83$, $p > 0.99$; WT social interaction versus *Shank3B*$^{-/-}$ + oxytocin social interaction, $t = 1.41$, $p > 0.99$; *Shank3B*$^{-/-}$ + vehicle social interaction versus *Shank3B*$^{-/-}$ + *L. reuteri*, $t = 0.82$, $p > 0.99$; *Shank3B*$^{-/-}$ + vehicle social interaction versus *Shank3B*$^{-/-}$ + *L. reuteri* social interaction, $t = 4.44$, $p < 0.01$; *Shank3B*$^{-/-}$ + vehicle social interaction versus *Shank3B*$^{-/-}$ + cocaine, $t = 4.03$, $p < 0.01$; *Shank3B*$^{-/-}$ + vehicle social interaction versus *Shank3B*$^{-/-}$ + oxytocin social interaction, $t = 4.72$, $p < 0.001$; *Shank3B*$^{-/-}$ + *L. reuteri* versus *Shank3B*$^{-/-}$ + *L. reuteri* social interaction, $t = 4.93$, $p < 0.001$; *Shank3B*$^{-/-}$ + *L. reuteri* versus *Shank3B*$^{-/-}$ + cocaine, $t = 4.55$, $p < 0.01$; *Shank3B*$^{-/-}$ + *L. reuteri* versus *Shank3B*$^{-/-}$ + oxytocin social interaction, $t = 5.19$, $p < 0.001$; *Shank3B*$^{-/-}$ + *L. reuteri* social interaction versus *Shank3B*$^{-/-}$ + cocaine, $t = 0.38$, $p > 0.99$; *Shank3B*$^{-/-}$ + *L. reuteri* social interaction versus *Shank3B*$^{-/-}$ + oxytocin social interaction, $t = 0.07$, $p > 0.99$; *Shank3B*$^{-/-}$ + cocaine versus *Shank3B*$^{-/-}$ + oxytocin social interaction, $t = 0.47$, $p > 0.99$; one-way ANOVA, $F_{7,46} = 16.68$, $p < 0.0001$). Representative AMPA and NMDA traces are shown above each group.

(C) Reciprocal social interaction was impaired in DA-*Oxtr*$^{-/-}$ mice, and neither *L. reuteri* or oxytocin reversed the social deficits in these mice (n = 10–12 pairs per group; Controls versus DA-*Oxtr*$^{-/-}$ + vehicle, $t = 6.095$, $p < 0.0001$; Controls versus DA-*Oxtr*$^{-/-}$ + *L. reuteri*, $t = 5.517$, $p < 0.0001$; Controls versus DA-*Oxtr*$^{-/-}$ + oxytocin, $t = 5.148$, $p < 0.0001$; DA-*Oxtr*$^{-/-}$ + vehicle versus DA-*Oxtr*$^{-/-}$ + *L. reuteri*, $t = 0.6059$, $p > 0.99$; DA-*Oxtr*$^{-/-}$ + vehicle versus DA-*Oxtr*$^{-/-}$ + oxytocin, $t = 0.8639$, $p > 0.99$; DA-*Oxtr*$^{-/-}$ + *L. reuteri* versus DA-*Oxtr*$^{-/-}$ + oxytocin, $t = 0.2712$, $p > 0.99$; one-way ANOVA, $F_{3,41} = 15.34$, $p < 0.0001$).

(D) AMPA/NMDA ratio of DA neurons in the lateral VTA at baseline and 24 hr after reciprocal social interaction (n = 6–7 per group; DA-*Oxtr*$^{-/-}$ + vehicle social interaction versus DA-*Oxtr*$^{-/-}$ social interaction + *L. reuteri*, $t = 0.02$, $p > 0.99$; DA-*Oxtr*$^{-/-}$ + vehicle social interaction versus Controls baseline, $t = 0.40$, $p > 0.99$; DA-*Oxtr*$^{-/-}$ + vehicle social interaction versus DA-*Oxtr*$^{-/-}$ + cocaine, $t = 5.47$, $p < 0.0001$; DA-*Oxtr*$^{-/-}$ + vehicle social interaction versus DA- *Oxtr*$^{-/-}$ + vehicle, $t = 0.44$, $p > 0.99$, DA-*Oxtr*$^{-/-}$ + vehicle social interaction versus Controls social interaction, $t = 4.92$, $p < 0.001$; DA-*Oxtr*$^{-/-}$ + vehicle social interaction versus DA-*Oxtr*$^{-/-}$ + oxytocin social interaction, $t = 0.089$, $p > 0.99$; DA-*Oxtr*$^{-/-}$ + *L. reuteri* social interaction versus Controls baseline, $t = 0.37$, $p > 0.99$; DA-*Oxtr*$^{-/-}$ + *L. reuteri* social interaction versus DA- *Oxtr*$^{-/-}$ + cocaine, $t = 5.49$, $p < 0.0001$; DA-*Oxtr*$^{-/-}$ + *L. reuteri* social interaction versus DA-*Oxtr*$^{-/-}$ + vehicle, $t = 0.47$,

*(legend continued on next page)*

modulate anxiety and depression-related behaviors via the vagus nerve (Bercik et al., 2011b; Bravo et al., 2011). Moreover, a recent report shows that optogenetic stimulation of the vagal gut-to-brain axis modulates reward-related behavior (Han et al., 2018), indicating that the vagus nerve connects the gut to the brain reward system. Coincidetally, we found that changes in the gut microbiome could influence long-lasting changes in synaptic efficacy in the mesolimbic dopamine reward system underlying social behaviors (Figure 7 and Buffington et al., 2016). In addition, here we provide new evidence that the vagus nerve is a central gut-brain communication pathway by which *L. reuteri* promote social behavior (Figures 4D–4F). While bacteria can interact with the vagus nerve via intrinsic primary afferent neurons (Perez-Burgos et al., 2014), further studies are necessary to investigate how precisely *L. reuteri* interacts with the vagus nerve. For instance, according to a recent report, cells from the gastrointestinal tract with a primarily endocrine function (enterodocrine cells) form synapses with vagal afferents (Kaelberer et al., 2018). It would be interesting to examine whether *L. reuteri* signals to the brain via alteration of the enterodocrine cell function or specifically by promoting synaptic function between these cells and vagal afferents.

Lastly, given that vagus nerve stimulation, like *L. reuteri* treatment, increases oxytocin levels (Stock and Uvnäs-Moberg, 1988) and transcutaneous vagus nerve stimulation enhances facial emotion recognition in humans (Sellaro et al., 2018), it would be interesting to examine in future experiments whether selective stimulation of vagal afferents improves social behaviors.

Fourth, to corroborate the validity of the microbial-based therapy, the effect of the probiotic treatment on behavior should be reproduced by other laboratories. Indeed, consistent with our results, an independent study by Tabouy et al. (2018) has recently found that *L. reuteri* successfully corrects social deficits in *Shank3B*$^{-/-}$ mice.

Finally, the microbial treatment must be safe and long-lasting in humans. While probiotics are generally believed to be safe, safety assessments (e.g., toxicity, genetic stability, and potential pathogenicity) of the microbial treatment of interest need to be performed. Accordingly, in terms of safety, an *L. reuteri* strain used in infants (Indrio et al., 2014) has received a certification of Generally Recognized as Safe (GRAS) for use in humans by the FDA. Moreover, when compared to (1) the transient effect on behavior associated with intranasal administration of oxytocin (Neumann et al., 2013; Peñagarikano et al., 2015), (2) the high amount of intranasal oxytocin needed to effective improve behavior in humans (Leng and Ludwig, 2016), and (3) the potential risk of oxytocin receptor desensitization (Robinson et al., 2003) associated with the long-term administaration of high dose of oxytocin, *L. reuteri* emerges an intriguing non-invasive therapeutic alternative to persistently increase "endogenous" oxytocin levels in the brain. Therefore, in view of the robust and consistent reversal of social behavioral deficits by *L. reuteri* in several ASD mouse models and its safety profile, it would be interesting to examine whether *L. reuteri* is able to improve social behavior in individuals with ASD in future studies.

## STAR★METHODS

Detailed methods are provided in the online version of this paper and include the following:

- KEY RESOURCES TABLE
- CONTACT FOR REAGENT AND RESOURCE SHARING
- EXPERIMENTAL MODEL AND SUBJECT DETAILS
  - Mice
- METHOD DETAILS
  - 16S rRNA Gene Sequencing
  - Bacterial Quantification by quantitative PCR (qPCR)
  - Culture and Treatment with *L. reuteri*
  - Three Chamber Social Test
  - Reciprocal Social Interaction
  - Open Field
  - Buried Food Test
  - Bilateral Subdiaphragmatic Vagotomy
  - Intestinal Permeability Assay
  - Gene Expression Analysis via Reverse Transcription followed by quantitative Polymerase Chain Reaction (RT-qPCR)
  - Oxytocin Administration
  - L-371,257 Administration
  - Immunofluorescence
  - Electrophysiology
  - Statistical Analysis

## SUPPLEMENTAL INFORMATION

Supplemental Information includes 15 figures and can be found with this article at https://doi.org/10.1016/j.neuron.2018.11.018.

## ACKNOWLEDGMENTS

We thank Marina Grasso for administrative support; Sanjeev Khatiwada and Andon N. Placzek for comments on the manuscript; Rebecca S. Blackwood, Alton Swennes, and Stephanie W. Fowler for veterinary advice; and Benjamin R. Arenkiel for providing the *Oxtr*$^{flox/flox}$ mice. This work was supported by funding from the NIH (R01 MH112356) and Sammons Enterprise to M.C.-M.

## AUTHOR CONTRIBUTIONS

M.S., S.W.D., S.A.B., and M.C.-M. designed the experiments. M.S., S.W.D., S.A.B., and M.B.F. performed the experiments. E.N.M. performed the surgery.

$p > 0.99$; DA-*Oxtr*$^{-/-}$ + *L. reuteri* social interaction versus Controls social interaction: $t = 4.94$, $p < 0.001$; Controls baseline versus DA-*Oxtr*$^{-/-}$ + cocaine, $t = 6.08$, $p < 0.0001$; Controls baseline versus DA-*Oxtr*$^{-/-}$ + vehicle, $t = 0.88$, $p > 0.99$; Controls baseline versus Controls social interaction, $t = 5.50$, $p < 0.0001$; Controls baseline versus DA-*Oxtr*$^{-/-}$ + oxytocin social interaction, $t = 0.32$, $p > 0.99$; DA-*Oxtr*$^{-/-}$ + cocaine versus DA-*Oxtr*$^{-/-}$ + vehicle, $t = 5.23$, $p < 0.001$; DA-*Oxtr*$^{-/-}$ + cocaine versus Controls social interaction, $t = 0.55$, $p > 0.99$; DA-*Oxtr*$^{-/-}$ + cocaine versus DA-*Oxtr*$^{-/-}$ + oxytocin social interaction, $t = 5.76$, $p < 0.0001$; DA-*Oxtr*$^{-/-}$ + vehicle versus Controls social interaction, $t = 4.66$, $p < 0.001$; DA-*Oxtr*$^{-/-}$ + vehicle versus DA-*Oxtr*$^{-/-}$ + oxytocin social interaction, $t = 0.55$, $p > 0.99$; Controls social interaction versus DA-*Oxtr*$^{-/-}$ + oxytocin social interaction, $t = 5.19$, $p < 0.001$; one-way ANOVA, $F_{6,38} = 13.46$, $p < 0.0001$). ns, not significant. Plots show mean ± SEM. See also Figures S12–S14.

M.S., S.W.D., and S.A.B. analyzed the data. M.S., S.W.D., and M.C.-M. wrote the manuscript with input from S.A.B and R.A.B.

## DECLARATION OF INTERESTS

The authors declare no competing interest. A patent application related to the findings has been filed by Baylor College of Medicine.

Received: July 9, 2018
Revised: September 18, 2018
Accepted: November 8, 2018
Published: December 3, 2018

## REFERENCES

American Psychiatric Association (2013). Diagnostic and Statistical Manual of Mental Disorders (DSM-5) (American Psychiatric Pub).

Arentsen, T., Raith, H., Qian, Y., Forssberg, H., and Diaz Heijtz, R. (2015). Host microbiota modulates development of social preference in mice. Microb. Ecol. Health Dis. *26*, 29719.

Baio, J., Wiggins, L., Christensen, D.L., Maenner, M.J., Daniels, J., Warren, Z., Kurzius-Spencer, M., Zahorodny, W., Robinson Rosenberg, C., White, T., et al. (2018). Prevalence of autism spectrum disorder among children aged 8 years—autism and developmental disabilities monitoring network, 11 Sites, United States, 2014. Morbidity and Mortality Weekly Report Surveillance Summaries (Washington, DC: 2002) 67, 1–23.

Bariselli, S., Tzanoulinou, S., Glangetas, C., Prévost-Solié, C., Pucci, L., Viguié, J., Bezzi, P., O'Connor, E.C., Georges, F., Lüscher, C., and Bellone, C. (2016). SHANK3 controls maturation of social reward circuits in the VTA. Nat. Neurosci. *19*, 926–934.

Benjamini, Y., Drai, D., Elmer, G., Kafkafi, N., and Golani, I. (2001). Controlling the false discovery rate in behavior genetics research. Behav. Brain Res. *125*, 279–284.

Bercik, P., Denou, E., Collins, J., Jackson, W., Lu, J., Jury, J., Deng, Y., Blennerhassett, P., Macri, J., McCoy, K.D., et al. (2011a). The intestinal microbiota affect central levels of brain-derived neurotropic factor and behavior in mice. Gastroenterology *141*, 599–609.

Bercik, P., Park, A.J., Sinclair, D., Khoshdel, A., Lu, J., Huang, X., Deng, Y., Blennerhassett, P.A., Fahnestock, M., Moine, D., et al. (2011b). The anxiolytic effect of Bifidobacterium longum NCC3001 involves vagal pathways for gut-brain communication. Neurogastroenterol. Motil. *23*, 1132–1139.

Bertola, A., Mathews, S., Ki, S.H., Wang, H., and Gao, B. (2013). Mouse model of chronic and binge ethanol feeding (the NIAAA model). Nat. Protoc. *8*, 627–637.

Borre, Y.E., O'Keeffe, G.W., Clarke, G., Stanton, C., Dinan, T.G., and Cryan, J.F. (2014). Microbiota and neurodevelopmental windows: implications for brain disorders. Trends Mol. Med. *20*, 509–518.

Bravo, J.A., Forsythe, P., Chew, M.V., Escaravage, E., Savignac, H.M., Dinan, T.G., Bienenstock, J., and Cryan, J.F. (2011). Ingestion of Lactobacillus strain regulates emotional behavior and central GABA receptor expression in a mouse via the vagus nerve. Proc. Natl. Acad. Sci. USA *108*, 16050–16055.

Buffington, S.A., Di Prisco, G.V., Auchtung, T.A., Ajami, N.J., Petrosino, J.F., and Costa-Mattioli, M. (2016). Microbial reconstitution reverses maternal diet-induced social and synaptic deficits in offspring. Cell *165*, 1762–1775.

Christensen, J., Grønborg, T.K., Sørensen, M.J., Schendel, D., Parner, E.T., Pedersen, L.H., and Vestergaard, M. (2013). Prenatal valproate exposure and risk of autism spectrum disorders and childhood autism. JAMA *309*, 1696–1703.

Coretti, L., Cristiano, C., Florio, E., Scala, G., Lama, A., Keller, S., Cuomo, M., Russo, R., Pero, R., Paciello, O., et al. (2017). Sex-related alterations of gut microbiota composition in the BTBR mouse model of autism spectrum disorder. Sci. Rep. *7*, 45356.

De Angelis, M., Piccolo, M., Vannini, L., Siragusa, S., De Giacomo, A., Serrazzanetti, D.I., Cristofori, F., Guerzoni, M.E., Gobbetti, M., and Francavilla, R. (2013). Fecal microbiota and metabolome of children with autism and pervasive developmental disorder not otherwise specified. PLoS ONE *8*, e76993.

Desbonnet, L., Clarke, G., Shanahan, F., Dinan, T.G., and Cryan, J.F. (2014). Microbiota is essential for social development in the mouse. Mol. Psychiatry *19*, 146–148.

Diaz Heijtz, R., Wang, S., Anuar, F., Qian, Y., Björkholm, B., Samuelsson, A., Hibberd, M.L., Forssberg, H., and Pettersson, S. (2011). Normal gut microbiota modulates brain development and behavior. Proc. Natl. Acad. Sci. USA *108*, 3047–3052.

Ding, H.T., Taur, Y., and Walkup, J.T. (2017). Gut microbiota and autism: key concepts and findings. J. Autism Dev. Disord. *47*, 480–489.

Dölen, G., Darvishzadeh, A., Huang, K.W., and Malenka, R.C. (2013). Social reward requires coordinated activity of nucleus accumbens oxytocin and serotonin. Nature *501*, 179–184.

Donaldson, Z.R., and Young, L.J. (2008). Oxytocin, vasopressin, and the neurogenetics of sociality. Science *322*, 900–904.

Edgar, R.C. (2010). Search and clustering orders of magnitude faster than BLAST. Bioinformatics *26*, 2460–2461.

Edgar, R.C. (2013). UPARSE: highly accurate OTU sequences from microbial amplicon reads. Nat. Methods *10*, 996–998.

Fåk, F., and Bäckhed, F. (2012). Lactobacillus reuteri prevents diet-induced obesity, but not atherosclerosis, in a strain dependent fashion in *Apoe*$^{-/-}$ mice. PLoS ONE *7*, e46837.

Falcinelli, S., Rodiles, A., Unniappan, S., Picchietti, S., Gioacchini, G., Merrifield, D.L., and Carnevali, O. (2016). Probiotic treatment reduces appetite and glucose level in the zebrafish model. Sci. Rep. *6*, 18061.

Golubeva, A.V., Joyce, S.A., Moloney, G., Burokas, A., Sherwin, E., Arboleya, S., Flynn, I., Khochanskiy, D., Moya-Pérez, A., Peterson, V., et al. (2017). Microbiota-related changes in bile acid and tryptophan metabolism are associated with gastrointestinal dysfunction in a mouse model of autism. EBioMedicine *24*, 166–178.

Gregory, R., Cheng, H., Rupp, H.A., Sengelaub, D.R., and Heiman, J.R. (2015). Oxytocin increases VTA activation to infant and sexual stimuli in nulliparous and postpartum women. Horm. Behav. *69*, 82–88.

Groppe, S.E., Gossen, A., Rademacher, L., Hahn, A., Westphal, L., Gründer, G., and Spreckelmeyer, K.N. (2013). Oxytocin influences processing of socially relevant cues in the ventral tegmental area of the human brain. Biol. Psychiatry *74*, 172–179.

Gunaydin, L.A., Grosenick, L., Finkelstein, J.C., Kauvar, I.V., Fenno, L.E., Adhikari, A., Lammel, S., Mirzabekov, J.J., Airan, R.D., Zalocusky, K.A., et al. (2014). Natural neural projection dynamics underlying social behavior. Cell *157*, 1535–1551.

Gupta, J., and Nebreda, A.R. (2014). Analysis of intestinal permeability in mice. Biol. Protoc. *4*, e1289.

Hallmayer, J., Cleveland, S., Torres, A., Phillips, J., Cohen, B., Torigoe, T., Miller, J., Fedele, A., Collins, J., Smith, K., et al. (2011). Genetic heritability and shared environmental factors among twin pairs with autism. Arch. Gen. Psychiatry *68*, 1095–1102.

Han, W., Tellez, L.A., Perkins, M.H., Perez, I.O., Qu, T., Ferreira, J., Ferreira, T.L., Quinn, D., Liu, Z.W., Gao, X.B., et al. (2018). A neural circuit for gut-induced reward. Cell *175*, 887–888.

Hara, Y., Ago, Y., Higuchi, M., Hasebe, S., Nakazawa, T., Hashimoto, H., Matsuda, T., and Takuma, K. (2017). Oxytocin attenuates deficits in social interaction but not recognition memory in a prenatal valproic acid-induced mouse model of autism. Horm. Behav. *96*, 130–136.

Harony-Nicolas, H., Kay, M., Hoffmann, J.D., Klein, M.E., Bozdagi-Gunal, O., Riad, M., Daskalakis, N.P., Sonar, S., Castillo, P.E., Hof, P.R., et al. (2017). Oxytocin improves behavioral and electrophysiological deficits in a novel Shank3-deficient rat. eLife *6*, e18904.

Holingue, C., Newill, C., Lee, L.C., Pasricha, P.J., and Daniele Fallin, M. (2018). Gastrointestinal symptoms in autism spectrum disorder: a review of the literature on ascertainment and prevalence. Autism Res. *11*, 24–36.

Holmes, J.L., Van Itallie, C.M., Rasmussen, J.E., and Anderson, J.M. (2006). Claudin profiling in the mouse during postnatal intestinal development and along the gastrointestinal tract reveals complex expression patterns. Gene Expr. Patterns *6*, 581–588.

Hsiao, E.Y., McBride, S.W., Hsien, S., Sharon, G., Hyde, E.R., McCue, T., Codelli, J.A., Chow, J., Reisman, S.E., Petrosino, J.F., et al. (2013). Microbiota modulate behavioral and physiological abnormalities associated with neurodevelopmental disorders. Cell *155*, 1451–1463.

Huang, Y.C., and Hessler, N.A. (2008). Social modulation during songbird courtship potentiates midbrain dopaminergic neurons. PLoS ONE *3*, e3281.

Huang, W., Placzek, A.N., Di Prisco, G.V., Khatiwada, S., Sidrauski, C., Krnjević, K., Walter, P., Dani, J.A., and Costa-Mattioli, M. (2016). Translational control by eIF2$\alpha$ phosphorylation regulates vulnerability to the synaptic and behavioral effects of cocaine. eLife *5*, e12052.

Human Microbiome Project Consortium (2012). Structure, function and diversity of the healthy human microbiome. Nature *486*, 207–214.

Hung, L.W., Neuner, S., Polepalli, J.S., Beier, K.T., Wright, M., Walsh, J.J., Lewis, E.M., Luo, L., Deisseroth, K., Dölen, G., and Malenka, R.C. (2017). Gating of social reward by oxytocin in the ventral tegmental area. Science *357*, 1406–1411.

Indrio, F., Di Mauro, A., Riezzo, G., Civardi, E., Intini, C., Corvaglia, L., Ballardini, E., Bisceglia, M., Cinquetti, M., Brazzoduro, E., et al. (2014). Prophylactic use of a probiotic in the prevention of colic, regurgitation, and functional constipation: a randomized clinical trial. JAMA Pediatr. *168*, 228–233.

Jiang, Y.H., and Ehlers, M.D. (2013). Modeling autism by SHANK gene mutations in mice. Neuron *78*, 8–27.

Jones-Davis, D.M., Yang, M., Rider, E., Osbun, N.C., da Gente, G.J., Li, J., Katz, A.M., Weber, M.D., Sen, S., Crawley, J., and Sherr, E.H. (2013). Quantitative trait loci for interhemispheric commissure development and social behaviors in the BTBR $T^{+}$ tf/J mouse model of autism. PLoS ONE *8*, e61829.

Joyner, K., Smith, G.P., and Gibbs, J. (1993). Abdominal vagotomy decreases the satiating potency of CCK-8 in sham and real feeding. Am. J. Physiol. *264*, R912–R916.

Julio-Pieper, M., Bravo, J.A., Aliaga, E., and Gotteland, M. (2014). Review article: intestinal barrier dysfunction and central nervous system disorders—a controversial association. Aliment. Pharmacol. Ther. *40*, 1187–1201.

Kaelberer, M.M., Buchanan, K.L., Klein, M.E., Barth, B.B., Montoya, M.M., Shen, X., and Bohórquez, D.V. (2018). A gut-brain neural circuit for nutrient sensory transduction. Science *361*, eaat5236.

Kawa, R., Saemundsen, E., Lóa Jónsdóttir, S., Hellendoorn, A., Lemcke, S., Canal-Bedia, R., García-Primo, P., and Moilanen, I. (2017). European studies on prevalence and risk of autism spectrum disorders according to immigrant status-a review. Eur. J. Public Health *27*, 101–110.

Kim, Y.S., and Leventhal, B.L. (2015). Genetic epidemiology and insights into interactive genetic and environmental effects in autism spectrum disorders. Biol. Psychiatry *77*, 66–74.

Kim, J.-W., Seung, H., Kim, K.C., Gonzales, E.L.T., Oh, H.A., Yang, S.M., Ko, M.J., Han, S.-H., Banerjee, S., and Shin, C.Y. (2017). Agmatine rescues autistic behaviors in the valproic acid-induced animal model of autism. Neuropharmacology *113* (Pt A), 71–81.

Leclercq, S., Mian, F.M., Stanisz, A.M., Bindels, L.B., Cambier, E., Ben-Amram, H., Koren, O., Forsythe, P., and Bienenstock, J. (2017). Low-dose penicillin in early life induces long-term changes in murine gut microbiota, brain cytokines and behavior. Nat. Commun. *8*, 15062.

Lee, H.-J., Caldwell, H.K., Macbeth, A.H., Tolu, S.G., and Young, W.S., 3rd (2008). A conditional knockout mouse line of the oxytocin receptor. Endocrinology *149*, 3256–3263.

Leng, G., and Ludwig, M. (2016). Intranasal oxytocin: myths and delusions. Biol. Psychiatry *79*, 243–250.

Lim, J.S., Lim, M.Y., Choi, Y., and Ko, G. (2017). Modeling environmental risk factors of autism in mice induces IBD-related gut microbial dysbiosis and hyperserotonemia. Mol. Brain *10*, 14.

LoParo, D., and Waldman, I.D. (2015). The oxytocin receptor gene (OXTR) is associated with autism spectrum disorder: a meta-analysis. Mol. Psychiatry *20*, 640–646.

Mayer, E.A., Padua, D., and Tillisch, K. (2014). Altered brain-gut axis in autism: comorbidity or causative mechanisms? BioEssays *36*, 933–939.

McElhanon, B.O., McCracken, C., Karpen, S., and Sharp, W.G. (2014). Gastrointestinal symptoms in autism spectrum disorder: a meta-analysis. Pediatrics *133*, 872–883.

McFarlane, H.G., Kusek, G.K., Yang, M., Phoenix, J.L., Bolivar, V.J., and Crawley, J.N. (2008). Autism-like behavioral phenotypes in BTBR T+tf/J mice. Genes Brain Behav. *7*, 152–163.

McMurdie, P.J., and Holmes, S. (2013). phyloseq: an R package for reproducible interactive analysis and graphics of microbiome census data. PLoS ONE *8*, e61217.

Melis, M.R., Melis, T., Cocco, C., Succu, S., Sanna, F., Pillolla, G., Boi, A., Ferri, G.L., and Argiolas, A. (2007). Oxytocin injected into the ventral tegmental area induces penile erection and increases extracellular dopamine in the nucleus accumbens and paraventricular nucleus of the hypothalamus of male rats. Eur. J. Neurosci. *26*, 1026–1035.

Methé, B.A., Nelson, K.E., Pop, M., Creasy, H.H., Giglio, M.G., Huttenhower, C., Gevers, D., Petrosino, J.F., Abubucker, S., Badger, J.H., et al.; Human Microbiome Project Consortium (2012). A framework for human microbiome research. Nature *486*, 215–221.

Meyza, K.Z., and Blanchard, D.C. (2017). The BTBR mouse model of idiopathic autism - Current view on mechanisms. Neurosci. Biobehav. Rev. *76* (Pt A), 99–110.

Neufeld, K.M., Kang, N., Bienenstock, J., and Foster, J.A. (2011). Reduced anxiety-like behavior and central neurochemical change in germ-free mice. Neurogastroenterol. Motil. *23*, 255–264.

Neumann, I.D., Maloumby, R., Beiderbeck, D.I., Lukas, M., and Landgraf, R. (2013). Increased brain and plasma oxytocin after nasal and peripheral administration in rats and mice. Psychoneuroendocrinology *38*, 1985–1993.

Olson, C.A., Vuong, H.E., Yano, J.M., Liang, Q.Y., Nusbaum, D.J., and Hsiao, E.Y. (2018). The gut microbiota mediates the anti-seizure effects of the ketogenic diet. Cell *173*, 1728–1741.

Ornoy, A. (2009). Valproic acid in pregnancy: how much are we endangering the embryo and fetus? Reprod. Toxicol. *28*, 1–10.

Owyang, C., and Heldsinger, A. (2011). Vagal control of satiety and hormonal regulation of appetite. J. Neurogastroenterol. Motil. *17*, 338–348.

Peça, J., Feliciano, C., Ting, J.T., Wang, W., Wells, M.F., Venkatraman, T.N., Lascola, C.D., Fu, Z., and Feng, G. (2011). Shank3 mutant mice display autistic-like behaviours and striatal dysfunction. Nature *472*, 437–442.

Pedersen, C.A., Caldwell, J.D., Walker, C., Ayers, G., and Mason, G.A. (1994). Oxytocin activates the postpartum onset of rat maternal behavior in the ventral tegmental and medial preoptic areas. Behav. Neurosci. *108*, 1163–1171.

Peñagarikano, O., Lázaro, M.T., Lu, X.H., Gordon, A., Dong, H., Lam, H.A., Peles, E., Maidment, N.T., Murphy, N.P., Yang, X.W., et al. (2015). Exogenous and evoked oxytocin restores social behavior in the Cntnap2 mouse model of autism. Sci. Transl. Med. *7*, 271ra8.

Perez-Burgos, A., Wang, B., Mao, Y.-K., Mistry, B., McVey Neufeld, K.A., Bienenstock, J., and Kunze, W. (2013). Psychoactive bacteria Lactobacillus rhamnosus (JB-1) elicits rapid frequency facilitation in vagal afferents. Am. J. Physiol. Gastrointest. Liver Physiol. *304*, G211–G220.

Perez-Burgos, A., Mao, Y.-K., Bienenstock, J., and Kunze, W.A. (2014). The gut-brain axis rewired: adding a functional vagal nicotinic "sensory synapse". FASEB J. *28*, 3064–3074.

Poutahidis, T., Kearney, S.M., Levkovich, T., Qi, P., Varian, B.J., Lakritz, J.R., Ibrahim, Y.M., Chatzigiagkos, A., Alm, E.J., and Erdman, S.E. (2013). Microbial symbionts accelerate wound healing via the neuropeptide hormone oxytocin. PLoS ONE *8*, e78898.

Quast, C., Pruesse, E., Yilmaz, P., Gerken, J., Schweer, T., Yarza, P., Peplies, J., and Glöckner, F.O. (2013). The SILVA ribosomal RNA gene database project: improved data processing and web-based tools. Nucleic Acids Res. *41*, D590–D596.

Robinson, C., Schumann, R., Zhang, P., and Young, R.C. (2003). Oxytocin-induced desensitization of the oxytocin receptor. Am. J. Obstet. Gynecol. *188*, 497–502.

Sabatier, N., Leng, G., and Menzies, J. (2013). Oxytocin, feeding, and satiety. Front. Endocrinol. (Lausanne) *4*, 35.

Scattoni, M.L., Gandhy, S.U., Ricceri, L., and Crawley, J.N. (2008). Unusual repertoire of vocalizations in the BTBR T+tf/J mouse model of autism. PLoS ONE *3*, e3067.

Schieve, L.A., Gonzalez, V., Boulet, S.L., Visser, S.N., Rice, C.E., Van Naarden Braun, K., and Boyle, C.A. (2012). Concurrent medical conditions and health care use and needs among children with learning and behavioral developmental disabilities, National Health Interview Survey, 2006-2010. Res. Dev. Disabil. *33*, 467–476.

Sellaro, R., de Gelder, B., Finisguerra, A., and Colzato, L.S. (2018). Transcutaneous vagus nerve stimulation (tVNS) enhances recognition of emotions in faces but not bodies. Cortex *99*, 213–223.

Sharon, G., Sampson, T.R., Geschwind, D.H., and Mazmanian, S.K. (2016). The central nervous system and the gut microbiome. Cell *167*, 915–932.

Silverman, J.L., Yang, M., Lord, C., and Crawley, J.N. (2010). Behavioural phenotyping assays for mouse models of autism. Nat. Rev. Neurosci. *11*, 490–502.

Stappenbeck, T.S., and Virgin, H.W. (2016). Accounting for reciprocal host-microbiome interactions in experimental science. Nature *534*, 191–199.

Stock, S., and Uvnäs-Moberg, K. (1988). Increased plasma levels of oxytocin in response to afferent electrical stimulation of the sciatic and vagal nerves and in response to touch and pinch in anaesthetized rats. Acta Physiol. Scand. *132*, 29–34.

Strati, F., Cavalieri, D., Albanese, D., De Felice, C., Donati, C., Hayek, J., Jousson, O., Leoncini, S., Renzi, D., Calabrò, A., and De Filippo, C. (2017). New evidences on the altered gut microbiota in autism spectrum disorders. Microbiome *5*, 24.

Sullivan, E.L., Nousen, E.K., and Chamlou, K.A. (2014). Maternal high fat diet consumption during the perinatal period programs offspring behavior. Physiol. Behav. *123*, 236–242.

Sun, J., Qiao, Y., Qi, C., Jiang, W., Xiao, H., Shi, Y., and Le, G.W. (2016). High-fat-diet-induced obesity is associated with decreased antiinflammatory Lactobacillus reuteri sensitive to oxidative stress in mouse Peyer's patches. Nutrition *32*, 265–272.

Suzuki, T. (2013). Regulation of intestinal epithelial permeability by tight junctions. Cell. Mol. Life Sci. *70*, 631–659.

Tabouy, L., Getselter, D., Ziv, O., Karpuj, M., Tabouy, T., Lukic, I., Maayouf, R., Werbner, N., Ben-Amram, H., Nuriel-Ohayon, M., et al. (2018). Dysbiosis of microbiome and probiotic treatment in a genetic model of autism spectrum disorders. Brain Behav. Immun. *73*, 310–319.

Tang, Y., Chen, Z., Tao, H., Li, C., Zhang, X., Tang, A., and Liu, Y. (2014). Oxytocin activation of neurons in ventral tegmental area and interfascicular nucleus of mouse midbrain. Neuropharmacology *77*, 277–284.

Tomova, A., Husarova, V., Lakatosova, S., Bakos, J., Vlkova, B., Babinska, K., and Ostatnikova, D. (2015). Gastrointestinal microbiota in children with autism in Slovakia. Physiol. Behav. *138*, 179–187.

Tyzio, R., Nardou, R., Ferrari, D.C., Tsintsadze, T., Shahrokhi, A., Eftekhari, S., Khalilov, I., Tsintsadze, V., Brouchoud, C., Chazal, G., et al. (2014). Oxytocin-mediated GABA inhibition during delivery attenuates autism pathogenesis in rodent offspring. Science *343*, 675–679.

Ungless, M.A., Whistler, J.L., Malenka, R.C., and Bonci, A. (2001). Single cocaine exposure in vivo induces long-term potentiation in dopamine neurons. Nature *411*, 583–587.

Uvnäs-Moberg, K., Handlin, L., and Petersson, M. (2015). Self-soothing behaviors with particular reference to oxytocin release induced by non-noxious sensory stimulation. Front. Psychol. *5*, 1529.

Vuong, H.E., and Hsiao, E.Y. (2017). Emerging roles for the gut microbiome in autism spectrum disorder. Biol. Psychiatry *81*, 411–423.

Vuong, H.E., Yano, J.M., Fung, T.C., and Hsiao, E.Y. (2017). The microbiome and host behavior. Annu. Rev. Neurosci. *40*, 21–49.

Wang, X., Wang, B.R., Zhang, X.J., Xu, Z., Ding, Y.Q., and Ju, G. (2002). Evidences for vagus nerve in maintenance of immune balance and transmission of immune information from gut to brain in STM-infected rats. World J. Gastroenterol. *8*, 540–545.

Xiao, L., Priest, M.F., Nasenbeny, J., Lu, T., and Kozorovitskiy, Y. (2017). Biased oxytocinergic modulation of midbrain dopamine systems. Neuron *95*, 368–384.e5.

Yang, M., and Crawley, J.N. (2009). Simple behavioral assessment of mouse olfaction. Curr. Protoc. Neurosci. *48*, 8.24.21–28.24.12.

Yang, M., Perry, K., Weber, M.D., Katz, A.M., and Crawley, J.N. (2011). Social peers rescue autism-relevant sociability deficits in adolescent mice. Autism Res. *4*, 17–27.

Zhang, T.A., Placzek, A.N., and Dani, J.A. (2010). In vitro identification and electrophysiological characterization of dopamine neurons in the ventral tegmental area. Neuropharmacology *59*, 431–436.

Zhang, Q., Widmer, G., and Tzipori, S. (2013). A pig model of the human gastrointestinal tract. Gut Microbes *4*, 193–200.

Zhang, M., Ma, W., Zhang, J., He, Y., and Wang, J. (2018). Analysis of gut microbiota profiles and microbe-disease associations in children with autism spectrum disorders in China. Sci. Rep. *8*, 13981.

Zhao, H., Tu, Z., Xu, H., Yan, S., Yan, H., Zheng, Y., Yang, W., Zheng, J., Li, Z., Tian, R., et al. (2017). Altered neurogenesis and disrupted expression of synaptic proteins in prefrontal cortex of SHANK3-deficient non-human primate. Cell Res. *27*, 1293–1297.

# STAR★METHODS

## KEY RESOURCES TABLE

| REAGENT or RESOURCE | SOURCE | IDENTIFIER |
|---|---|---|
| Antibodies | | |
| Oxytocin Antibody | ImmunoStar | Cat# 20068; RRID:AB_572258 |
| Anti-NeuN | Millipore | Cat# MAB377; RRID:AB_2298772 |
| VECTASHIELD Mounting Medium with DAPI antibody | Vector Laboratories | Cat# H-1200; RRID:AB_2336790 |
| Goat anti-rabbit Alexa Fluor 488 | ThermoFisher Scientific | Cat# R37116; RRID:AB_2556544 |
| Goat anti-mouse Alexa Fluor 594 | ThermoFisher Scientific | Cat# A-21125; RRID:AB_2535767 |
| Bacterial and Virus Strains | | |
| *Lactobacillus reuteri* MM4 | Provided by Robert A. Britton Laboratory | N/A |
| Chemicals, Peptides, and Recombinant Proteins | | |
| Isofluorane | Henry Schein Animal Health | Cat# 029405 |
| Oxytocin | Tocris Bioscience | Cat# 1910 |
| L-371,257 | Tocris Bioscience | Cat# 2410 |
| Paraformaldehyde | Sigma-Aldrich | Cat# P6148 |
| CCK-8 | Sigma-Aldrich | Cat# C2175 |
| FITC-Dextran 4KDa | Sigma-Aldrich | Cat# FD4 |
| Triton X-100 | Bio-Rad | Cat# 1610407 |
| Dimethyl sulfoxide (DMSO) | Sigma-Aldrich | Cat# 472301 |
| Picrotoxin | Sigma-Aldrich | Cat# P1675 |
| DL-APV Sodium Salt | Tocris Bioscience | Cat# 3693 |
| Valproic Acid | Sigma-Aldrich | Cat#P4543 |
| SR-Buprenorphine | ZooPharm | *Cat# BZ8069317* |
| Cocaine hydrochloride | Sigma Aldrich | Cat# C5776 |
| Gelatine from bovin skin | Sigma Aldrich | Cat# G9391 |
| Critical Commercial Assays | | |
| MO BIO PowerSoil DNA Isolation Kit | MO BIO Laboratories | Cat# 12888 |
| DNeasy Blood&Tissue Kit | Quiagen | Cat# 69504 |
| RNeasy Plus Universal Minikit | Quiagen | Cat# 73404 |
| Superscript VILO cDNA synthesis kit | Invitrogen (ThermoFhisher Scientific) | Cat# 11754050 |
| Experimental Models: Organisms/Strains | | |
| *Shank3B*$^{+/-}$ mice | The Jackson Laboratory | Cat# 017688 |
| C57BL/6J mice | The Jackson Laboratory | Cat# 000664 |
| BTBR mice | The Jackson Laboratory | Cat# 002282 |
| DAT-Cre mice | The Jackson Laboratory | Cat# 020080 |
| *Oxtr*$^{fl/fl}$ | Benjamin R. Arenkiel laboratory | Lee et al., 2008 |
| GF mice | Center for Comparative Medicine (CCM) of Baylor College of Medicine | N/A |
| Oligonucleotides | | |
| L. reuteri primers: Forward, 5′GAAGATCAGTCGCAYTGGCCCAA-3′; Reverse, 5′-TCCATTGTGGCCGATCAG-3′ | Sigma-Aldrich | Sun et al., 2016 |
| General bacteria primers: Forward, 5′-ACTCCTACGGGAGGCAGCAG-3′; Reverse, 5′-ATTACCGCGGCTGCTGG-3′ | Sigma-Aldrich | Sun et al., 2016 |

(*Continued on next page*)

*Continued*

| REAGENT or RESOURCE | SOURCE | IDENTIFIER |
|---|---|---|
| *Cdh1* primers: 5′-TCCTTGTTCGGCTATGTGTC-3′, 5′-GGCATGCACCTAAGAATCAG-3′ | Sigma-Aldrich | Holmes et al., 2006 |
| *Cldn5*: 5′-GTGGAACGCTCAGATTTCAT-3′, 5′-TGGACATTAAGGCAGCATCT-3′ | Sigma-Aldrich | Holmes et al., 2006 |
| *Ocln* primers: 5′-GCTGTGATGTGTGTGAGCTG-3′, 5′-GACGGTCTACCTGGAGGAAC-3′ | Sigma-Aldrich | Holmes et al., 2006 |
| *Jam1* primers: 5′-ACCCTCCCTCCTTTCCTAC-3′, 5′-CTAGGACTCTTGCCCAATCC-3′ | Sigma-Aldrich | Holmes et al., 2006 |
| *Actb* primers: 5′-CTCTTCCAGCCTTCCTTCCT-3′, 5′-TGCTAGGGCTGTGATCTCCT-3′ | Sigma-Aldrich | Holmes et al., 2006 |
| Software and Algorithms | | |
| Anymaze | Stoelting | https://www.stoeltingco.com/anymaze/video-tracking/software.html |
| AxioVision | Carl Zeiss Microimaging | https://www.zeiss.com/microscopy/us/downloads/axiovision-downloads.html |
| Graphpad Prism 7.0 | Graphpad Software | http://www.graphpad.com/ |
| Adobe Illustrator CS6 | Adobe | N/A |
| Adobe Photoshop CS6 | Adobe | N/A |
| FLUOstar OPTIMA | BMG LABTECH | https://www.bmglabtech.com/downloads/ |
| pClamp 10 | Molecular Device | N/A |
| USEARCH v7.0.1090 | Edgar, 2010 | N/A |
| ImageJ | NIH | https://imagej.nih.gov/ij/download.html |
| Miseq Software | Illumina | https://support.illumina.com/sequencing/sequencing_software/miseq_reporter/downloads.html |
| StepOne Software | Applied Biosystem (Life Technology-ThermoFisher Scientific) | http://www.thermofisher.com/us/en/home/technical-resources/software-downloads/StepOne-and-StepOnePlus-Real-Time-PCR-System.html |

## CONTACT FOR REAGENT AND RESOURCE SHARING

Further information and requests for resources and reagents should be directed to and will be fulfilled by the Lead Contact, Mauro Costa-Mattioli (costamat@bcm.edu).

## EXPERIMENTAL MODEL AND SUBJECT DETAILS

### Mice

C57BL/6J, *Shank3B*$^{+/-}$ mice, DAT-cre mice, and BTBR mice were obtained from Jackson Laboratories (Bar Harbor, ME) and *Oxtr*$^{flox/flox}$ mice were previously described (Lee et al., 2008). *Shank3B*$^{-/-}$ mice were generated from *Shank3B*$^{+/-}$ x *Shank3B*$^{+/-}$ breeding and littermates were cohoused according to sex. DA-*Oxtr*$^{-/-}$ (DAT-cre, *Oxtr*$^{fl/fl}$) mice were generated by crossing DAT-cre mice to *Oxtr*$^{fl/fl}$ mice and cohoused by genotype and sex. All mice were kept on a 12 hr light/dark cycle and had access to food and water *ad libitum*. Germ-free (GF) mice (C57BL/6J background) were housed in a flexible isolator fed with HEPA-filtered air and provided with irradiated food and water at the Baylor College of Medicine gnobiotic facility. The VPA mice were generated by administrating a single dose of valproic acid sodium salt (Sigma Aldrich) to a pregnant C57BL/6J female at embryonic day 12.5 (Lim et al., 2017). The offspring from either vehicle-injected or VPA-injected females were used as control and VPA mice respectively. For all the mouse models, only male mice were included in the study and at least two litters were used for each experiment. Animal care and experimental procedures were approved by Baylor College of Medicine's Institutional Animal Care and Use Committee in accordance with all guidelines set forth by the U.S. National Institutes of Health.

## METHOD DETAILS

### 16S rRNA Gene Sequencing

16S rRNA gene sequencing was performed as previously described (Buffington et al., 2016). Methods were adapted from protocols provided for the NIH-Human Microbiome Project (Methé et al., 2012; Human Microbiome Project Consortium, 2012). Bacterial genomic DNA was extracted using MO BIO PowerSoil DNA Isolation Kit (MO BIO Laboratories). The 16S rDNA V4 region was amplified by PCR and sequenced in the MiSeq platform (Illumina) using the 2x250 bp paired-end protocol yielding pair-end reads that overlap almost completely. The primers used for amplification contain adapters for MiSeq sequencing and single-end barcodes allowing pooling and direct sequencing of PCR products. The 16S rRNA gene read pairs were demultiplexed based on the unique molecular barcodes, and reads were merged using USEARCH v7.0.1090 (Edgar, 2010), allowing zero mismatches and a minimum overlap of 50 bases. Merged reads were trimmed at first base with Q5. A quality filter was applied to the resulting merged reads. Reads containing above 0.05 expected errors were discarded. 16S rRNA gene sequences were clustered into Operational Taxonomic Units (OTUs) at a similarity cutoff value of 97% using the UPARSE algorithm (Edgar, 2013). OTUs were mapped to an optimized version of the SILVA Database (Quast et al., 2013) containing only the 16S v4 region to determine taxonomies. Abundances were recovered by mapping the demultiplexed reads to the UPARSE OTUs. A custom script constructed a rarefied OTU table from the output files generated in the previous two steps for downstream analyses of alpha-diversity, beta-diversity, and phylogenetic trends.

### Bacterial Quantification by quantitative PCR (qPCR)

DNA was isolated from fecal pellets using DNeasy Blood & Tissue Kit (QIAGEN), according to the manufacturer's protocol. The concentration of DNA isolated from each pellet was obtained via NanoDrop. qPCR was performed using PowerUp SYBR Green Master Mix, according to the manufacturer's protocol (Applied Biosystems, Carlsbad, USA) with primer sets targeting the 16S ribosomal subunit of *L. reuteri* and of all bacteria (see key resources table).

### Culture and Treatment with *L. reuteri*

*Lactobacillus reuteri* MM4-1A (ATCC-PTA-6475) was cultured aerobically in MRS broth at 37°C. Briefly, cultures were centrifuged, washed, resuspended in phosphate buffered saline (PBS), and frozen at −80°C until use. PBS (vehicle) or *L. reuteri* were added to the drinking water daily to minimize dosage variability. The experimental group received live bacteria ($\sim$1x$10^8$ organisms/mouse/day), while the control group received equal volume of PBS. Mice consumed the treated water *ad libitum* for the duration of the treatment period. Fecal sample collection, behavioral assays, tissue collection and electrophysiological recordings were initiated 4 weeks after treatment began.

### Three Chamber Social Test

All behavioral tests were assayed on 7- to 10-week-old male mice. Social behaviors were performed as previously described (Buffington et al., 2016; Silverman et al., 2010). Briefly, mice were first habituated for a 10 minutes in an empty 60 × 40 × 23 cm Plexiglass arena divided into three interconnected chambers (left, center, right). Sociability was evaluated during a second 10-minutes period in which the subject could interact either with an empty wire cup (Empty) or a wire cup containing a genotype, age, sex and treatment-matched stranger conspecific (Mouse 1). The interaction time was determined by measuring the time the subject mouse spent sniffing or climbing upon either the empty cup or the cup containing the stranger mouse. The position of the empty cup/stranger mouse in the left or right chamber during the sociability period was counterbalanced between trials, in order to avoid bias. Preference for social novelty was assayed, in a third 10 minutes period, by introducing a second stranger mouse (Mouse 2) into the previously the empty wire cup. The time spent interacting with the empty cup or mouse 1 or mouse 2 was recorded and measured using the automated AnyMaze software by trained, independent observers. The human observers were blind to the treatment group.

### Reciprocal Social Interaction

Mice were placed in a 25 × 25 × 25 cm Plexiglass neutral arena with an unfamiliar conspecific matched according genotype, age, sex and treatment. Trained, independent observers recorded the time a pair of mice socially interacted, using the AnyMaze software. This included close following, touching, nose-to-nose sniffing, nose-to-anus sniffing, grooming and/or crawling over/under each other. The human observers were blind to the treatment group.

### Open Field

Mice were placed in an open arena (40 × 40 × 20 cm) and allowed to explore freely for 10 minutes and their position was continually monitored using the tracking software AnyMaze. Distance traveled, speed, and time spent in the center of the arena were recorded and automatically measured throughout the task. The center of the arena was defined as the interior 20 × 20 cm area.

### Buried Food Test

To examine olfactory abilities we used the buried food test as previoiulsy described (Yang and Crawley, 2009). Briefly, mice were food-deprived for 24 hr before the test. A small platable cookie (Nabisco, Teddy Graham) was buried 1 cm beneath the surface of a 3 cm bedding and the time the animal took to locate the buried cookie was recorded. Faillure to use odor cues to locate the buried food during this test is an indication of impaired olfaction.

### Bilateral Subdiaphragmatic Vagotomy

Mice were habituated to a liquid diet (35% sweetened condensed milk in water) for two days before surgery and fasted overnight before surgery. Anesthesia was delivered by gaseous isoflurane (Henry Schein Animal Health) in an induction chamber and then through a nose piece of the stereotaxic apparatus (Leica Biosystems). The surgical site was shaved and wiped with betadine and alcohol three times before a midline laparotomy was made. The liver and small intestine were gently retracted to visualize the stomach and lower esophagus. Both vagus nerve trunks were dissected off the esophagus and all neural and connective tissue surrounding the esophagus (below the diaphragm) were removed to ensure that all vagus branches were transected. A separate group of mice had a sham operation in which the vagus nerve was visualized, but not dissected. Incisions were closed with 5-0 absorbable suture (i.e., vicryl on a taper needle) and the skin was closed with a non-absorbable suture 5-0 on a cutting needle (i.e., Nylon or prolene) to re-approximate the abdominal wall musculature and skin. Histoacryl or similar surgical glue was applied over the incision to ensure that the closure was watertight. Sustained release buprenorphine (1mg/kg) was administered 1 hr prior to the start of surgery. A second dose of sustained release buprenorphine was administered subcutaneously at 72 hr after the initial dosing. After the surgery was complete, animals were allowed to recover from surgery and anesthesia in a clean cage half-positioned on a heat pad and returned to the animal facility after they were alert and demonstrated no complications from the procedure. In order to avoid ileus, the mice were fed with the same liquid diet for 3 days after surgery. Finally, before giving the mice the regular pellet diet, they were fed with a fully fortified gel diet (DietGel 31M, Clear$H_2O$) for two days in order to facilitate a full recovery. Animals were monitored daily for at least 1 week to ensure complete recovery from surgery.

To assess the completeness of the vagotomy we performed the satiety test. Satiety induced by CCK-8 is mediated by the vagus nerve (Owyang and Heldsinger, 2011). The completeness of the vagotomy was determined by analyzing the satiety effect induced by CCK-8 (Sigma–Aldrich) administration, following 20 hr of food deprivation. Briefly, mice were fasted overnight. The following day sham operated and vagotomized mice were single housed and treated with an intraperitoneal injection (i.p.) of CCK-8 (dissolved in 0.1% PBS) at a dose of 8 μg/kg body weight (Bravo et al., 2011). Food intake was monitored for the following 2 hr, by weighing food pellets pre- and post-test. The completeness of the vagotomy was made at the end of the experiment, at least two weeks after the final treatment dose, since probiotics have been shown to influence the satiety effect of CCK-8 (Fåk and Bäckhed, 2012; Falcinelli et al., 2016).

### Intestinal Permeability Assay

The intestinal permeability procedure was adapted from a previously described protocol (Gupta and Nebreda, 2014). Briefly, colitis was induced in control mice by adding 3% dextran sulfate sodium salt (DSS; Sigma Aldrich) in drinking water for 7 days. Control and experimental mice were then fasted overnight and weighted the next morning. Mice were administered FITC-dextran (4KDa, Sigma Aldrich, 44 mg/100 g of body weight) by oral gavage, as described (Bertola et al., 2013). After 4 hr, mice were anesthetized and blood was collected (300-400 μl) by cardiac puncture. Serum was extracted from whole blood by allowing the sample to clot undisturbed at room temperature for 15–30 minutes and then centrifuged at 3000 x g for 15 minutes at 4°C. The resulting supernatant (serum) was transferred into a clean polypropylene tube and then diluted with an equal volume of PBS and 100 μL of diluted serum to a 96-well microplate in duplicate. FITC concentration in serum was determined by spectrofluorometry (FLUOstar OPTIMA, BMG LABTECH) with an excitation of 485 nm (20 nm band width) and an emission wavelength of 528 nm (20 nm band width) using as standard serially diluted FITC-dextran (0, 125, 250, 500, 1,000, 2,000, 4,000, 6,000, 8,000 ng/ml).

### Gene Expression Analysis via Reverse Transcription followed by quantitative Polymerase Chain Reaction (RT-qPCR)

The total RNA was extracted from gut tissue using the RNeasy Plus Universal Minikit (QIAGEN). cDNA was generated using SuperScript VILO (Invitrogen). qPCR was performed using PowerUp SYBR Green Master Mix, according to the manufacturer's protocol (Applied Biosystems, Carlsbad, USA) to quantify relative expression levels of the tight junction related genes *Cdh1*, *Ocln*, *Cldn5*, and *Jam1*. Expression of the mouse *β-actin* was used to normalize each gene expression levels. Primer sequences are provided in the Key Resources Table.

### Oxytocin Administration

Oxytocin (Tocris Bioscience) was administrated intranasally at a dose of 200 mg/kg as previously reported (Buffington et al., 2016). Briefly, oxytocin was dissolved in 10% dimethyl sulfoxide (DMSO) in PBS and 10% DMSO in PBS was used as the vehicle control. 1.25 μL of vehicle or oxytocin were administrated into each nostril from P10 pipette 30 minutes prior social behavior test, since the effects of oxytocin last 2 hr with this delivery method (Peñagarikano et al., 2015), resulting in elevated brain concentration for about 90 minutes (Neumann et al., 2013).

### L-371,257 Administration

L-371,257 (Tocris Bioscience) was administrated intranasally at a dose of ~300 μg/kg, as previously reported (Peñagarikano et al., 2015). Briefly, L-371,257 was dissolved in 10% dimethyl sulfoxide (DMSO) in PBS and 10% DMSO in PBS was used as the vehicle control. Two microliters of L-371,257 (or vehicle) were administrated into each nostril 20 minutes prior to reciprocal social interaction test.

## Immunofluorescence

Immunofluorescence was performed as we previously described (Buffington et al., 2016). Briefly, mice were deeply anesthetized by inhalation of isoflurane and perfused through the ascending aorta with 10 mL 0.9% PBS followed by 30 mL 4% paraformaldehyde (PFA) in 0.1M phosphate buffer (PB). Brains were removed, immersed in the same fixative overnight at 4°C and subsequently cryoprotected in 30% sucrose (in 0.1M PB) over 3 days. Coronal sections were cut at 30 μm with a cryostat (Leica Biosystem) and then collected in ice-cold PBS. Slices were rinsed in 0.1M PB, blocked with 5% normal goat serum, 0.3% Triton X-100 0.1M PB (PBTgs) for 1 hr rocking at RT, and then incubated for 24 hr at 4°C in a mixture of primary antibodies diluted in PBTgs. Sections were then washed (three times with 0.3% Triton X-100 0.1M PB) and incubated in a mixture of secondary antibodies coupled to a fluorochrome and diluted in PBTgs for 1.5–2 hr in the dark at room temperature. Sections were washed again (three times with PBTgs, 0.1M PB and 0.05M PB respectively for five minutes each). Slices were mounted onto 2% gelatin-coated slides (Sigma-Aldrich), air-dried, and coverslipped with a mounting medium [Fluorescence Vectashield H-1200 with DAPI (Vector Labs)]. Primary antibodies used were rabbit anti-oxytocin (ImmunoStar, 1:2000 dilution), mouse anti-NeuN (Millipore, 1:2000 dilution), while secondary antibodies were goat anti-rabbit Alexa Fluor 488 (ThermoFisher Scientific) and goat anti-mouse Alexa Fluor 594 (ThermoFisher Scientific, 1:1000 dilution), respectively.

Fluorescent imaging and data acquisition were performed on a Zeiss AxioImager Z2 microscope (Car Zeiss MicroImaging) mounted with an AxioCam digital camera (Carl Zeiss MicroImaging). Images were captured using AxioVision acquisition software (Carl Zeiss MicroImaging). All images within the same set of experiments were acquired at identical exposure times, for every channel used, to allow for comparison of fluorescence intensity. Hypothalamic oxytocin-expressing neurons and NeuN-expressing cells number were assessed in the well-defined PVN region using the automatic cell counter plugin in ImageJ, as previously described (Buffington et al., 2016), using the following operational sequence: (1) open image file, (2) 16-bit conversion 3) subtract background, (3) adjust threshold, (4) watershed, (5) analyze particles. Automatic identification of cell boundaries was validated against the source image. Fluorescence intensity was measured in ImageJ by selecting regions of interest (i.e., Oxytocin- and NeuN-positive hypothalamic cell bodies, 30 cells per mouse) using the following operational sequence: (1) open image file, (2) 16-bit conversion, (3) set measurement, (4) ROI manager, (5) measure. Contrast and brightness were linearly adjusted using Photoshop (Adobe) or ImageJ (NIH) uniformally across all images within the dataset.

## Electrophysiology

Recordings were performed as previously described (Buffington et al., 2016; Huang et al., 2016), with minor modifications. Briefly, animals were anaesthetized with isoflurane and then decapitated. The brain was rapidly removed from the skull and fixed on a vibroslicer stage (VT 1000S, Leica Microsystems, Buffalo Grove, IL) with cyano-acrylic glue. Acute 220-300 μm-thick coronal slices were cut in ice-cold (2-3°C) cutting-solution containing the following (in mM): 87 NaCl, 25 $NaHCO_3$, 25 glucose, 75 sucrose, 2.5 KCl, 1.25 $NaH_2PO_4$, 0.5 $CaCl_2$ and 7 $MgCl_2$ (equilibrated with 95% $O_2$–5% $CO_2$ gas mixture, pH 7.3-7.5). Slices were incubated for 20 minutes at 32°C and then stored at room temperature in a holding bath containing oxygenated standard artificial cerebrospinal fluid (ACSF) containing (in mM): 125 NaCl, 25 NaHCO3, 25 glucose, 2.5 KCl, 1.25 NaH2PO4, 2 CaCl2, and 1 MgCl2 (equilibrated with 95% $O_2$-5% $CO_2$), for at least 40 minutes, before being transferred to a recording chamber mounted on the stage of an upright microscope (Examiner D1, Carl Zeiss, Oberkochen, Germany). The slices were perfused with oxygenated ACSF (2 ml/min) containing the $GABA_A$ receptor antagonist picrotoxin (100 μM; Sigma-Aldrich, USA) and maintained at 32°C with a Peltier feedback device (TC-324B, Warner Instrument). Whole-cell recordings were performed using conventional patch-clamp techniques. Patch pipettes were pulled from borosilicate glass capillaries (World Precision Instruments, Inc., FL) and filled with following intracellular solution (in mM): 117 $CsMeSO_3$, 0.4 EGTA, 20 HEPES, 2.8 NaCl, 2.5 Mg-ATP, and 0.25 Na-GTP; 5 TEA Cl, pH was adjusted to 7.3 and osmolarity to 290 mOsm using a vapor pressure osmometer Vapro*5600* (ELITechGroup Wescor, South Logan, Utah, *USA).* When filled with the intracellular solution, patch pipettes had a resistance of 2.0-3.0 MΩ before seal formation.

Recordings were performed with Multiclamp 700B (Molecular Devices), sampled at 20 kHz with Digidata 1440A (Molecular Device) interface, filtered online at 3 kHz with a Bessel low-pass filter and analyzed offline with pClamp10 software (Molecular Devices). Ventral tegmental area (VTA) was visually identified by infrared differential interference contrast video microscopy and lateral VTA was located considering the medial lemniscus and the medial terminal nucleus of the accessory optic tract as anatomical landmarks. Dopaminergic (DA) neurons in this area were identified evaluating the following features: 1) cells firing at a frequency of 1-5 Hz and the spike width > 1ms in cell attached configuration, 2) membrane capacitance (Cm) > 28 pF and 3) the presence of an Ih current and a leak current > 150 pA, when hyperpolarized from −40 mV to −120 in 10 mV steps (Bariselli et al., 2016; Zhang et al., 2010). Passive electrode-cell parameters were monitored throughout the experiments, analyzing passive current relaxations induced by 10 mV hyperpolarizing steps applied at the beginning of every trace. Variation of series resistance ($R_s$) > 20% led to the rejection of the experiment. AMPAR/NMDAR ratios were calculated as previously described (Buffington et al., 2016; Huang et al., 2016). Briefly, neurons were slowly voltage clamped at +40 mV until the holding current stabilized (at 200 pA). Monosynaptic Excitatory Post Synaptic currents (EPSCs) were evoked at 0.05 Hz with a bipolar stimulating electrode placed 50–150 μm rostral to the lateral VTA. After recording the dual-component EPSC, DL-AP5 (100 μM) was bath-applied for 10 minutes to isolate the AMPAR current, blocking the NMDAR. The NMDAR component was then obtained by offline subtraction of the AMPAR component from the original EPSC. The peak

amplitudes of the isolated components were used to calculate the AMPAR/NMDAR ratios. Cocaine hydrochloride (Sigma-Aldrich, St. Louis, MO) was dissolved in 0.9% saline and injected I.P. at a volume of 5 ml/kg 24 hr prior to electrophysiological recordings.

### Statistical Analysis

Statistical analysis was performed as described (Buffington et al., 2016). Data were presented as mean ± SEM. Statistical analyses performed include Mann-Whitney test, one- or two-way ANOVA with Bonferroni post hoc analysis to correct for multiple comparisons, unless otherwise indicated. p, *t*, and F values were presented in the figure legends. $p < 0.05$ was considered statistically significant. *$p < 0.05$, **$p < 0.01$, ***$p < 0.001$, ****$p < 0.0001$. GraphPad's Prism 6 (La Jolla, CA) software was used to perform statistical analyses and generate graphical data representations. As per 16S rRNA gene sequencing, analysis was conducted in RStudio 0.99.292 (http://www.R-project.org/ [2014]), utilizing the phyloseq package (McMurdie and Holmes, 2013) to import sample data and calculate alpha and beta-diversity metrics. 16S rRNA gene sequencing data was analyzed using Silva 115 and 123 (Quast et al., 2013). Analyses were performed on datasets that were rarefied 1,000x, then averaged and rounded. Significance of categorical variables were determined using the non-parametric Mann-Whitney test for two category comparisons or the Kruskal-Wallis test when comparing three or more categories. Correlation between two continuous variables was determined by linear regressions, where p values indicate the probability that the slope of the regression line is zero. Principal coordinate plots employed the Monte Carlo permutation test to estimate p values. All p values were adjusted for multiple comparisons with the FDR algorithm (Benjamini et al., 2001).